

Complete next-to-next-to-leading order QCD corrections to the decay matrix in B -meson mixing at leading power

Ulrich Nierste^a, Pascal Reeck^a, Vladyslav Shtabovenko^b, and Matthias Steinhauser^a

^a*Institut für Theoretische Teilchenphysik,
Wolfgang-Gaede Straße 1, Karlsruhe Institute of Technology (KIT)
76131 Karlsruhe, Germany*

^b*Theoretische Physik 1, Center for Particle Physics Siegen,
Universität Siegen, 57068 Siegen, Germany*

ABSTRACT: We compute next-to-next-to-leading order corrections to the decay width difference of mass eigenstates and the charge-parity (CP) asymmetry a_{fs} in flavour-specific decays of neutral B mesons. We include both current-current and penguin operators at three-loop order. All input integrals in the transition amplitude are reduced to a small set of master integrals which depend on the ratio of the charm and bottom quark masses. The latter are computed using semi-analytic methods which provide deep expansions around properly selected values of m_c/m_b . We provide numerical results for $\Delta\Gamma$ and $\Delta\Gamma/\Delta M$, both for the B_d and B_s system, including a detailed uncertainty analysis. Using the experimental value for the mass difference ΔM_s we predict $\Delta\Gamma_s = (0.078 \pm 0.015) \text{ ps}^{-1}$. For the CP asymmetries we find $a_{\text{fs}}^s = (2.27 \pm 0.13) \times 10^{-5}$ and $a_{\text{fs}}^d = -(5.19 \pm 0.30) \times 10^{-4}$. Furthermore, we show that the ratios $(\Delta\Gamma_s/\Delta M_s)/(\Delta\Gamma_d/\Delta M_d)$ and $\Delta\Gamma_d/\Delta\Gamma_s$ can be predicted with high precision. The former quantity permits the prediction $\Delta\Gamma_d = (0.00215 \pm 0.00013) \text{ ps}^{-1}$ from the measurements of $\Delta M_{d,s}$ and $\Delta\Gamma_s$. We further discuss the impact of $\Delta\Gamma_d/\Delta\Gamma_s$ on the CKM unitarity triangle and present ready-to-use formulae which permit improved predictions once updated results for the operator matrix elements are available.

Contents

1	Introduction	1
2	General formalism	7
3	Amplitude generation	10
4	Phenomenology	11
4.1	$\Delta\Gamma_q$ and $\Delta\Gamma_q/\Delta M_q$	12
4.1.1	B_s system	12
4.1.2	B_d system	15
4.2	a_{fs}^q	16
4.3	The double ratio $((\Delta\Gamma_d/\Delta M_d)/(\Delta\Gamma_s/\Delta M_s))$	17
4.4	Unitarity triangle constraints from a_{fs}^d and $\Delta\Gamma_d/\Delta\Gamma_s$	20
4.5	Numerical results independent of CKM values and hadronic matrix elements	25
5	Conclusions	26

1 Introduction

B_d and B_s mesons mix with their antiparticles via box diagrams involving two W bosons. As a consequence, a meson tagged as B_q , where $q = d$ or $q = s$, at time $t = 0$ evolves into a superposition of B_q and \bar{B}_q for $t > 0$. The time evolution of this coupled system reads

$$i \frac{d}{dt} \begin{pmatrix} |B_q(t)\rangle \\ |\bar{B}_q(t)\rangle \end{pmatrix} = \left(M^q - i \frac{\Gamma^q}{2} \right) \begin{pmatrix} |B_q(t)\rangle \\ |\bar{B}_q(t)\rangle \end{pmatrix}. \quad (1.1)$$

$M^q = M^{q\dagger}$ and $\Gamma^q = \Gamma^{q\dagger}$ are the 2×2 mass and decay matrix, respectively, and $B_q - \bar{B}_q$ mixing occurs because the off-diagonal elements M_{12}^q and Γ_{12}^q are non-zero. The initial conditions for the time-dependent states are $|B_q(0)\rangle = |B_q\rangle$ and $|\bar{B}_q(0)\rangle = |\bar{B}_q\rangle$. By

diagonalising $M^q - i\Gamma^q/2$ one finds the mass eigenstates $|B_{q,L}(t)\rangle$ and $|B_{q,H}(t)\rangle$ which obey exponential decay laws,

$$|B_{q,L}(t)\rangle = |B_{q,L}\rangle e^{-iM_L^q t - \Gamma_L^q t/2}, \quad |B_{q,H}(t)\rangle = |B_{q,H}\rangle e^{-iM_H^q t - \Gamma_H^q t/2}.$$

The labels refer to “light” and “heavy” and the exponentials involve the masses and widths of the two eigenstates. One can perform the diagonalisation with the ansatz

$$|B_{q,L}\rangle = p|B_q\rangle + q|\bar{B}_q\rangle, \quad |B_{q,H}\rangle = p|B_q\rangle - q|\bar{B}_q\rangle, \quad \text{where } |p|^2 + |q|^2 = 1. \quad (1.2)$$

$B_q - \bar{B}_q$ mixing is a $\Delta B = 2$ transition, meaning that the beauty quantum number changes by two units. These transitions are characterised by four theoretical quantities which are

$$|M_{12}^q|, \quad |\Gamma_{12}^q|, \quad \phi_q = \arg\left(-\frac{\Gamma_{12}^q}{M_{12}^q}\right), \quad (1.3)$$

and the relative phase between M_{12}^q and the amplitude of a chosen b quark decay [1]. For the latter usually $b \rightarrow c\bar{c}s$ is taken and within the Standard Model (SM) the corresponding mixing-induced CP asymmetry in $B_d(t) \rightarrow J/\psi K_S$ permits the experimental determination of the angle $\beta = \arg(-V_{cd}V_{cb}^*/(V_{td}V_{tb}^*))$ of the standard unitarity triangle of the Cabibbo-Kobayashi-Maskawa (CKM) matrix V . The counterpart for $B_s - \bar{B}_s$ mixing is $B_s(t) \rightarrow J/\psi\phi$, measuring the angle $\beta_s = \arg(-V_{cs}^*V_{cb}/(V_{ts}^*V_{tb}))$ of a “squashed” unitarity triangle in the SM. The three quantities in Eq. (1.3) universally affect all decays of neutral B_q mesons and are related to three phenomenological quantities as

$$\begin{aligned} \Delta M_q &\equiv M_H^q - M_L^q = 2|M_{12}^q|, \\ \Delta\Gamma_q &\equiv \Gamma_L^q - \Gamma_H^q = 2|\Gamma_{12}^q| \cos\phi_q, \\ a_{\text{fs}}^q &\equiv -\frac{|\Gamma_{12}^q|}{|M_{12}^q|} \sin\phi_q = \text{Im}\frac{\Gamma_{12}^q}{M_{12}^q}. \end{aligned} \quad (1.4)$$

Furthermore, we introduce

$$\frac{\Delta\Gamma_q}{\Delta M_q} = -\text{Re}\frac{\Gamma_{12}^q}{M_{12}^q}. \quad (1.5)$$

The quantity a_{fs}^q is the CP asymmetry in flavour-specific decays, characterised by the feature that $B_q \rightarrow f$ is allowed while $\bar{B}_q \rightarrow f$ is forbidden. The corresponding CP asymmetry reads

$$\frac{\Gamma(\bar{B}_q(t) \rightarrow f) - \Gamma(B_q(t) \rightarrow \bar{f})}{\Gamma(\bar{B}_q(t) \rightarrow f) + \Gamma(B_q(t) \rightarrow \bar{f})} = a_{\text{fs}}^q + a_{\text{CP}}^{\text{dir}}. \quad (1.6)$$

In Refs. [2, 3] it is explained how one can disentangle a_{fs}^q from the direct CP asymmetry $a_{\text{CP}}^{\text{dir}}$ by e.g. studying the untagged rate. In Eqs. (1.4) and (1.6) we have neglected corrections of order $|\Gamma_{12}^q/M_{12}^q|^2 \sim 10^{-5}$ or $\text{Im}[\Gamma_{12}^q/M_{12}^q] \lesssim 10^{-3}$ and will do so throughout this paper.

ΔM_q , which equals the $B_q - \bar{B}_q$ mixing oscillation frequency, and the CP phases $\beta_{(s)}$ determine the magnitude and phase of M_{12}^q but are insensitive to Γ_{12}^q . These quantities have different sensitivities to new physics and Γ_{12}^q is e.g. interesting to probe b decays into final states with new invisible particles [4].

The theory predictions of $\Delta\Gamma_q$ and a_{fs}^q all involve the decay matrix element Γ_{12}^q . To calculate M_{12}^q or Γ_{12}^q one employs an operator product expansion (OPE) separating the short-distance physics described by perturbatively calculable Wilson coefficients from the long-distance dynamics contained in hadronic operator matrix elements calculated by non-perturbative methods such as lattice gauge theory. Yet the calculation of Γ_{12}^q differs from the one of M_{12}^q in two important aspects: Firstly, Γ_{12}^q involves an expansion in powers of Λ_{QCD}/m_b , the *Heavy Quark Expansion* (HQE), where $\Lambda_{\text{QCD}} \sim 400$ MeV is the fundamental scale of QCD with new operators and coefficients in each power of Λ_{QCD}/m_b [5]. Secondly, the QCD corrections to Γ_{12}^q are governed by $\alpha_s(m_b)$, which is about twice as large as $\alpha_s(m_t)$ entering the perturbative series for M_{12}^q . In this paper we present the complete NNLO corrections to the leading-power term of Γ_{12}^q . In the phenomenological applications we need the ratio Γ_{12}^q/M_{12}^q and the NLO result for M_{12}^q is sufficient to match the NNLO precision of Γ_{12}^q .

For the calculation of Γ_{12}^q one first employs the weak $|\Delta B| = 1$ Hamiltonian $\mathcal{H}_{\text{eff}}^{|\Delta B|=1}$ obtained by integrating out top quark and W boson,

$$\mathcal{H}_{\text{eff}}^{|\Delta B|=1} = \mathcal{H}_{\text{cc}}^{|\Delta B|=1} + \mathcal{H}_{\text{peng}}^{|\Delta B|=1}, \quad (1.7)$$

which describes the weak interaction in terms of effective dimension-six operators with the two terms containing current-current and penguin operators, respectively. The former are four-quark operators describing W -mediated tree-level decays and QCD corrections to it. $\mathcal{H}_{\text{peng}}^{|\Delta B|=1}$ involves four additional four-quark operators and the chromomagnetic operator. We can safely neglect higher-order electroweak corrections, which would add more operators to $\mathcal{H}_{\text{peng}}^{|\Delta B|=1}$. The Wilson coefficients of the current-current operators have been calculated to next-to-leading order (NLO) in Refs. [6, 7] and to next-to-next-to-leading order (NNLO) in Refs. [8]. The chromomagnetic operator is proportional to the strong coupling, so that we will only need the corresponding NLO coefficient [9, 10] for our NNLO prediction of Γ_{12}^q . Since Γ_{12}^q involves $|\Delta B| = 2$ transitions, it is generated at second order of $\mathcal{H}_{\text{eff}}^{|\Delta B|=1}$:

$$\Gamma_{12}^q = \frac{1}{2M_{B_s}} \text{Abs}\langle B_q | i \int d^4x T \mathcal{H}_{\text{eff}}^{\Delta B=1}(x) \mathcal{H}_{\text{eff}}^{\Delta B=1}(0) | \bar{B}_q \rangle, \quad (1.8)$$

where “Abs” denotes the absorptive part of the matrix element. The contribution to Γ_{12}^q with two current-current

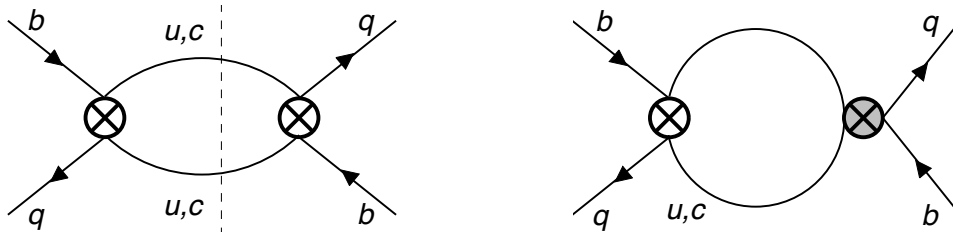


Figure 1: Leading-order diagrams contributing to Γ_{12}^q with two current-current operators (left) and one current-current and one penguin operator (right). Γ_{12}^q originates from decays into final states into which both B_q and \bar{B}_q can decay, indicated by the dashed line in the left figure.

insertions,

$$\Gamma_{12cc}^q = \frac{1}{2M_{B_s}} \text{Abs}\langle B_q | i \int d^4x T \mathcal{H}_{cc}^{\Delta B=1}(x) \mathcal{H}_{cc}^{\Delta B=1}(0) | \bar{B}_q \rangle, \quad (1.9)$$

is shown in the left diagram of Fig. 1. The HQE expresses Γ_{12cc}^q as a linear combination of local dimension-six $\Delta B = 2$ operators whose LO Wilson coefficients are found by matching the diagrams of Fig. 1 to the tree-level matrix elements of these operators. For the leading power of the $1/m_b$ expansion we need two physical $\Delta B = 2$ operators. Their hadronic matrix elements are the only non-perturbative quantities need for the predictions of $\Delta\Gamma_q$ and a_{fs}^q .

The leading-power contribution to Γ_{12cc}^q has been calculated to NLO in Ref. [11–13]. This calculation involves two-loop diagrams with one extra gluon compared to Fig. 1 as well as one-loop matrix elements of the $\Delta B = 2$ operators and results in $\mathcal{O}(\alpha_s)$ corrections to the desired $\Delta B = 2$ matching coefficients. Subsequently NNLO corrections have been calculated to order $\alpha_s^2 n_f$, where $n_f = 5$ is the number of active quarks, [14–16] and finally completely to order α_s^2 [3, 17]. These calculations involve expansions in the quark mass ratio m_c/m_b and the result of Ref. [3] with matching coefficients up to order $(m_c/m_b)^{20}$ constitutes our final NNLO prediction of Γ_{12cc}^q .

$\mathcal{H}_{\text{peng}}^{|\Delta B|=1}$ contributes less to Γ_{12}^q than $\mathcal{H}_{cc}^{|\Delta B|=1}$ because the numerical size of the Wilson coefficients of four-quark penguin operators is smaller as compared to the four-quark current ones, and the chromomagnetic penguin operator is proportional to α_s . The second-largest contribution to Γ_{12}^q is therefore

$$\Gamma_{12cp}^q = \frac{1}{M_{B_s}} \text{Abs}\langle B_q | i \int d^4x T \mathcal{H}_{cc}^{\Delta B=1}(x) \mathcal{H}_{\text{peng}}^{\Delta B=1}(0) | \bar{B}_q \rangle, \quad (1.10)$$

subsuming the interference effects of $\mathcal{H}_{cc}^{|\Delta B|=1}$ and $\mathcal{H}_{\text{peng}}^{|\Delta B|=1}$, with the LO contribution depicted in the right diagram of Fig. 1. The NLO contribution with a chromomagnetic operator to Γ_{12cp}^q involves only a one-loop diagram and is included in the result of Ref. [11].

The NLO calculation of $\Gamma_{12\,cp}^q$ including four-quark penguin operators has been performed in Ref. [18] to order $(m_c/m_b)^2$. Ref. [19] contains the NNLO contribution to $\Gamma_{12\,cp}^q$ involving one chromomagnetic operator.

The third contribution to Γ_{12}^q is

$$\Gamma_{12\,pp}^q = \frac{1}{2M_{B_s}} \text{Abs}\langle B_q | i \int d^4x T \mathcal{H}_{\text{peng}}^{\Delta B=1}(x) \mathcal{H}_{\text{peng}}^{\Delta B=1}(0) | \bar{B}_q \rangle. \quad (1.11)$$

While $\Gamma_{12\,cp}^q$ contributes to both $\Delta\Gamma_q$ and a_{fs}^q , this is not the case for $\Gamma_{12\,pp}^q$, which does not affect a_{fs}^q . This is because $\Gamma_{12\,pp}^q$ and M_{12}^q have the same CKM factor, so that $\text{Im}(\Gamma_{12\,pp}^q/M_{12}^q) = 0$ in Eq. (1.5). The $\alpha_s n_f$ terms and the complete NLO corrections to $\Gamma_{12\,pp}^q$ have been calculated in Refs. [15] and [19], respectively, both to order $(m_c/m_b)^2$. The latter reference also contains two-loop contributions with one or two insertions of the chromomagnetic operator, which go beyond NNLO. Finally we mention that the $1/m_b$ power corrections are only calculated to LO of QCD [13, 20, 21] and furthermore involve so-far poorly known hadronic matrix elements [22].

In this paper, we present the complete NLO and NNLO calculation of the leading-power terms in $\Gamma_{12\,cp}^q$ and $\Gamma_{12\,pp}^q$, which includes a deep expansion in m_c/m_b and novel three-loop results for diagrams with two insertions of four-quark penguin operators. To appreciate the first point we remark that $a_{\text{fs}}^q \propto (m_c/m_b)^2$, so that a precise prediction calls for an expansion of Γ_{12}^q beyond $(m_c/m_b)^2$. The NNLO prediction of $\Delta\Gamma_s$ in Ref. [3] has a theoretical uncertainty of the same size as the current experimental error, so that improvement is desirable. With the inclusion of the missing penguin contributions we aim at decreasing this uncertainty, which we estimate from the renormalisation scale dependence.

The phenomenological role of the four quantities $\Delta\Gamma_q$ and a_{fs}^q with $q = d$ or s is very different: The experimentally well-determined ratio $\Delta\Gamma_s/\Delta M_s$ is essentially independent of all CKM parameters, including the controversial $|V_{cb}|$, and therefore directly probes the SM [3, 17]. The SM prediction for a_{fs}^s is too small to ever be measured, but can be two orders of magnitude larger in the presence of new physics [13]. Future precise measurements of a_{fs}^d and $\Delta\Gamma_d$ will provide novel constraints of the apex $(\bar{\rho}, \bar{\eta})$ of the CKM unitarity triangle (UT). We define the CKM combinations

$$\lambda_u^q = V_{uq}^* V_{ub}, \quad \lambda_c^q = V_{cq}^* V_{cb}, \quad \lambda_t^q = V_{tq}^* V_{tb}, \quad (1.12)$$

and recall

$$\begin{aligned} -\frac{\lambda_u^d}{\lambda_c^d} &= R_u e^{-i\gamma} = \bar{\rho} - i\bar{\eta}, \\ -\frac{\lambda_t^d}{\lambda_c^d} &= R_t e^{i\beta} = 1 - \bar{\rho} + i\bar{\eta}, \end{aligned}$$

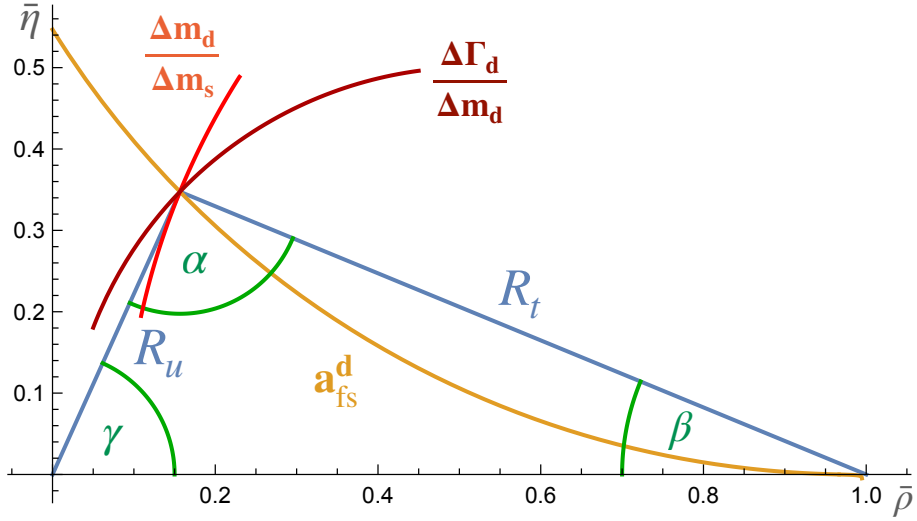


Figure 2: CKM unitarity triangle with constraints from $B-\bar{B}$ mixing observables.

$$-\frac{\lambda_u^d}{\lambda_t^d} = \frac{R_u}{R_t} e^{i\alpha} = 1 - \frac{e^{-i\beta}}{R_t} = \frac{-\bar{\rho}(1-\bar{\rho}) + \bar{\eta}^2 + i\bar{\eta}}{(1-\bar{\rho})^2 + \bar{\eta}^2}, \quad (1.13)$$

which involves angles and sides of the UT shown in Fig. 2. The constraint from a_{fs}^d has already been discussed in Refs. [3, 12], and Fig. 2 further shows the orthogonal constraint from $\Delta\Gamma_d/\Delta M_d$. The dominant contribution to this quantity comes with the same QCD corrections as $\Delta\Gamma_s/\Delta M_s$ and the hadronic matrix elements are the same up to $SU(3)_F$ breaking corrections. Furthermore, the CKM factor $\text{Re}(\lambda_u^d/\lambda_t^d)$ is proportional to $\cos\alpha$ (see Eq. (1.13)), which the global SM fit to the UT determines close to 0, so the linear and quadratic terms of this ratio in $\Delta\Gamma_d/\Delta M_d$ are negligible. Similarly, the quantity $\text{Re}(\lambda_u^s/\lambda_t^s)$ is tiny (see, e.g., Eq. (73) of Ref. [3]), so there is no substantial difference in $\Delta\Gamma/\Delta M$ across the B_s and B_d systems stemming from the CKM factors. These features allow us to predict the double ratio $\Delta\Gamma_d\Delta M_s/(\Delta M_d\Delta\Gamma_s)$ with high precision. Since three of the four involved quantities are already measured precisely, the future determination of $\Delta\Gamma_d$ will provide us with an excellent test of the SM from the double ratio.

The paper is organised as follows: In the next section we present the effective Hamiltonian and the operators used in this paper. Furthermore, we discuss in detail the numerical result for the $1/m_b$ -suppressed contributions as extracted from the literature. Section 4 is dedicated to phenomenology and discusses the quantities $\Delta\Gamma_q$, a_{fs}^q and $\Delta\Gamma_q/\Delta M_q$ for the B_s and B_d systems. We provide NNLO corrections including a detailed uncertainty analysis. Furthermore, NNLO predictions for the double ratio $(\Delta\Gamma_s/\Delta M_s)/(\Delta\Gamma_d/\Delta M_d)$ are discussed. Finally, we construct $\Delta\Gamma_d/\Delta\Gamma_s$ and discuss its complementary to a_{fs}^d for

providing constraints on the CKM unitarity triangle. We summarise our findings in Section 5.

2 General formalism

The $|\Delta B| = 1$ Hamiltonian in the CMM operator basis [23] reads

$$\begin{aligned} \mathcal{H}_{\text{eff}}^{|\Delta B|=1} = \frac{4G_F}{\sqrt{2}} & \left[-\lambda_t^q \left(\sum_{i=1}^6 C_i Q_i + C_8 Q_8 \right) - \lambda_u^q \sum_{i=1}^2 C_i (Q_i - Q_i^u) \right. \\ & \left. + V_{uq}^* V_{cb} \sum_{i=1}^2 C_i Q_i^{cu} + V_{cq}^* V_{ub} \sum_{i=1}^2 C_i Q_i^{uc} \right] + \text{h.c.}, \end{aligned} \quad (2.1)$$

where G_F is the Fermi constant and

$$\begin{aligned} Q_1^u &= \bar{q}_L \gamma_\mu T^a u_L \bar{u}_L \gamma^\mu T^a b_L, & Q_2^u &= \bar{q}_L \gamma_\mu u_L \bar{u}_L \gamma^\mu b_L, \\ Q_1^{cu} &= \bar{q}_L \gamma_\mu T^a u_L \bar{c}_L \gamma^\mu T^a b_L, & Q_2^{cu} &= \bar{q}_L \gamma_\mu u_L \bar{c}_L \gamma^\mu b_L, \\ Q_1^{uc} &= \bar{q}_L \gamma_\mu T^a c_L \bar{u}_L \gamma^\mu T^a b_L, & Q_2^{uc} &= \bar{q}_L \gamma_\mu c_L \bar{u}_L \gamma^\mu b_L, \\ Q_1 &= \bar{q}_L \gamma_\mu T^a c_L \bar{c}_L \gamma^\mu T^a b_L, & Q_2 &= \bar{q}_L \gamma_\mu c_L \bar{c}_L \gamma^\mu b_L, \\ Q_3 &= \bar{q}_L \gamma_\mu b_L \sum_{q'} \bar{q}' \gamma^\mu q', & Q_4 &= \bar{q}_L \gamma_\mu T^a b_L \sum_{q'} \bar{q}' \gamma^\mu T^a q', \\ Q_5 &= \bar{q}_L \gamma_{\mu_1} \gamma_{\mu_2} \gamma_{\mu_3} b_L \sum_{q'} \bar{q}' \gamma^{\mu_1} \gamma^{\mu_2} \gamma^{\mu_3} q', & Q_6 &= \bar{q}_L \gamma_{\mu_1} \gamma_{\mu_2} \gamma_{\mu_3} T^a b_L \sum_{q'} \bar{q}' \gamma^{\mu_1} \gamma^{\mu_2} \gamma^{\mu_3} T^a q', \\ Q_8 &= \frac{g_s}{16\pi^2} m_b \bar{q}_L \sigma^{\mu\nu} T^a b_R G_{\mu\nu}^a. \end{aligned} \quad (2.2)$$

Here $q_L = P_L q$ with $P_L = (1 - \gamma_5)/2$, $\sigma^{\mu\nu} = i[\gamma^\mu, \gamma^\nu]/2$, and T^a is the generator of $\text{SU}(3)_c$.

It helps to write Γ_{12}^q as

$$\Gamma_{12}^q = -(\lambda_c^q)^2 \Gamma_{12}^{cc} - 2\lambda_c^q \lambda_u^q \Gamma_{12}^{uc} - (\lambda_u^q)^2 \Gamma_{12}^{uu} \quad (2.3)$$

$$= -(\lambda_t^q)^2 \left[\Gamma_{12}^{cc} + 2 \frac{\lambda_u^q}{\lambda_t^q} (\Gamma_{12}^{cc} - \Gamma_{12}^{uc}) + \left(\frac{\lambda_u^q}{\lambda_t^q} \right)^2 (\Gamma_{12}^{uu} + \Gamma_{12}^{cc} - 2\Gamma_{12}^{uc}) \right]. \quad (2.4)$$

with real coefficients Γ_{12}^{ab} multiplying the three possible CKM factors. The current-current contributions in Fig. 1 match Eq. (2.3) such that $a, b = u, c$ correspond to the quarks on the internal lines. In the step from Eq. (2.3) to Eq. (2.4) we have used $\lambda_c^q = -\lambda_t^q - \lambda_u^q$ to get an expression best suited to normalise Γ_{12}^q to M_{12}^q , which is proportional to $(\lambda_t^q)^2$. The penguin operators in $\mathcal{H}_{\text{eff}}^{|\Delta B|=1}$ are proportional to λ_t^q . Terms quadratic in the penguin coefficients contribute to all three Γ^{ab} 's in Eq. (2.3) but only to the first term in the square

bracket of Eq. (2.4). The second term in this square bracket receives contributions from the interference of penguin and current-current operators.

The individual contributions in Eq. (2.4) evaluate to [3]

$$\Gamma_{12}^{ab} = \frac{G_F^2 m_b^2}{24\pi M_{B_q}} \left[H^{ab}(\bar{z}) \langle B_q | Q | \bar{B}_q \rangle + \tilde{H}_S^{ab}(\bar{z}) \langle B_q | \tilde{Q}_S | \bar{B}_q \rangle \right] + \Gamma_{12,1/m_b}^{ab} \quad (2.5)$$

with two matrix elements of dimension-six $\Delta B = 2$ operators,

$$\begin{aligned} Q &= 4 (\bar{s}^c \gamma^\mu P_L b^c) (\bar{s}^d \gamma_\mu P_L b^d), \\ \tilde{Q}_S &= 4 (\bar{s}^c P_R b^d) (\bar{s}^d P_R b^c), \end{aligned} \quad (2.6)$$

where $P_R = (1 + \gamma_5)/2$ and c, d are colour indices. The mass ratio $\bar{z} = [m_c(\mu_b)/m_b(\mu_b)]^2$ involves the charm and bottom masses in the $\overline{\text{MS}}$ scheme, both defined in five-flavour QCD, M_{B_q} is the B_q meson mass, and G_F is the Fermi constant. The calculation of the Wilson coefficients $H^{ab}(\bar{z})$ and $\tilde{H}_S^{ab}(\bar{z})$ for $ab = cc, uc, uu$ at NNLO of QCD is the subject of this paper.

$\Gamma_{12,1/m_b}^{ab}$ comprises power corrections of order Λ_{QCD}/m_b which have been calculated at LO of QCD in Ref. [20], NLO results are not available yet. As a first step to NLO, the mixing of dimension-seven operators into dimension-six operators under renormalization has been recently calculated in Ref. [24]. Since LO Λ_{QCD}/m_b -terms will finally dominate the theoretical uncertainties of our predictions, we present $\Gamma_{12,1/m_b}^{ab}$ here in a way which allows the reader to include future improvements of the calculation of the hadronic matrix elements entering $\Gamma_{12,1/m_b}^{ab}$. $\Gamma_{12,1/m_b}^{ab}$ involves seven dimension-seven operators commonly denoted by R_0, R_k , and \tilde{R}_k with $k = 1, 2, 3$. Their definitions can be found in Refs. [13, 20, 22].

Defining $r_j^q \equiv \langle B_q | R_j | \bar{B}_q \rangle$ and $\tilde{r}_j^q \equiv \langle B_q | \tilde{R}_j | \bar{B}_q \rangle$ one finds

$$\Gamma_{12,1/m_b}^{ab} = \frac{G_F^2 m_b^2}{24\pi M_{B_q}} \left[g_0^{ab} r_0^q + \sum_{j=1}^3 [g_j^{ab} r_j^q + \tilde{g}_j^{ab} \tilde{r}_j^q] \right] \quad (2.7)$$

with the coefficients $g_j^{ab}, \tilde{g}_j^{ab}$ (subsuming the results of Refs. [12, 20, 21]) defined in Ref. [13].

Estimating the uncertainties of $g_j^{ab}, \tilde{g}_j^{ab}$ from their μ -dependence in the interval [2.1 GeV, 8.4 GeV], we quote our central values for the scale $\mu_1 = 4.2$ GeV and the matching scale $\mu_0 = 165$ GeV of the weak effective Hamiltonian, finding

$$\begin{aligned} \Gamma_{12,1/m_b}^{cc} &= \frac{G_F^2 m_b^2}{24\pi M_{B_q}} [(-0.42 \pm 0.07)r_0^q + (0.84 \pm 0.14)r_1^q - (2.58 \pm 0.27)\tilde{r}_1^q \\ &\quad + (0.85 \pm 0.15)r_2^q - (2.62 \pm 0.28)\tilde{r}_2^q + (0.03 \pm 0.01)r_3^q - (0.09 \pm 0.01)\tilde{r}_3^q] \end{aligned} \quad (2.8)$$

$$= \begin{cases} - \left(\frac{m_b}{4.48 \text{ GeV}} \right)^2 7.77 \text{ ps}^{-1} (1 \pm 0.09)_{\text{scale}} (1 \pm 0.49)_{\text{mat. el.}} & \text{for } q = s \\ - \left(\frac{m_b}{4.48 \text{ GeV}} \right)^2 5.18 \text{ ps}^{-1} (1 \pm 0.10)_{\text{scale}} (1 \pm 0.52)_{\text{mat. el.}} & \text{for } q = d \end{cases} \quad (2.9)$$

$$\begin{aligned} 2(\Gamma_{12,1/m_b}^{cc} - \Gamma_{12,1/m_b}^{uc}) &= \\ & \frac{G_F^2 m_b^2}{24\pi M_{B_q}} [(0.007 \pm 0.001)r_0^q - (0.015 \pm 0.003)r_1^q + (0.046 \pm 0.005)\tilde{r}_1^q \\ & \quad + (0.001 \pm 0.000)r_2^q - (0.004 \pm 0.000)\tilde{r}_2^q + (0.032 \pm 0.005)r_3^q \\ & \quad - (0.099 \pm 0.010)\tilde{r}_3^q] \\ &= - \left(\frac{m_b}{4.48 \text{ GeV}} \right)^2 0.2099 \text{ ps}^{-1} (1 \pm 0.07)_{\text{scale}} (1 \pm 0.33)_{\text{mat. el.}} \quad \text{for } q = d \end{aligned} \quad (2.10)$$

$$\begin{aligned} \Gamma_{12,1/m_b}^{uu} + \Gamma_{12,1/m_b}^{cc} - 2\Gamma_{12,1/m_b}^{uc} &= \\ & \frac{G_F^2 m_b^2}{24\pi M_{B_q}} [(0.001 \pm 0.000)r_0^q - (0.001 \pm 0.000)r_1^q + (0.004 \pm 0.000)\tilde{r}_1^q \\ & \quad + (0.001 \pm 0.000)r_2^q - (0.002 \pm 0.000)\tilde{r}_2^q + (0.004 \pm 0.001)r_3^q \\ & \quad - (0.013 \pm 0.001)\tilde{r}_3^q] \\ &= - \left(\frac{m_b}{4.48 \text{ GeV}} \right)^2 0.0031 \text{ ps}^{-1} (1 \pm 0.08)_{\text{scale}} (1 \pm 0.33)_{\text{mat. el.}} \quad \text{for } q = d \end{aligned} \quad (2.11)$$

The numerical result in Eq. (2.9) is found with the hadronic matrix elements calculated for $q = s$ in Ref. [22]; their uncertainties combine to the value indicated by “mat. el.” which dominates over the scale uncertainty from the coefficients in Eq. (2.8). The small scale uncertainties in the last lines of Eqs. (2.9) to (2.11) result from partial cancellations between the different terms and underestimate the uncertainty from missing higher-order terms of the perturbation series. Still, even if one adds the quoted scale uncertainties of the coefficients in quadrature, one finds the uncertainty stemming from matrix elements significantly larger.

There are only five independent matrix elements due to relations like $r_2^q = -\tilde{r}_2^q(1 + \mathcal{O}(1/m_b, \alpha_s))$. Those matrix elements which are not available for $q = d$ are obtained by rescaling their $q = s$ counterparts with $f_{B_d}^2 M_{B_d}^2 / (f_{B_s}^2 M_{B_s}^2)$ and in the case of R_1 and \tilde{R}_1 also by m_d/m_s . The largest corrections to $\Delta\Gamma_q$ stem from $\Gamma_{12,1/m_b}^{cc}$ in Eq. (2.9), which

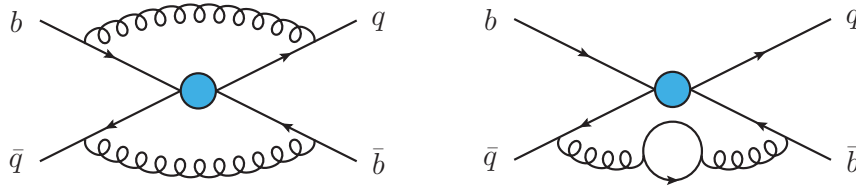


Figure 3: Two-loop Feynman diagrams of the $\Delta B = 2$ transition operator. The blue dot stands for the insertion of one of the operators Q , \tilde{Q}_S or R_0 .

is dominated by r_2^q , \tilde{r}_2^q , and r_0^q . The terms in Eqs. (2.10) and (2.11) give negligible contributions to $\Delta\Gamma_q$. For a_{fs}^q one instead needs the second term of Eq. (2.4), because the first term does not contribute to $\text{Im}(\Gamma_{12}^q/M_{12}^q)$. Since better lattice results will be available by the time experiments can probe the SM prediction for a_{fs}^s , we only provide numerical results for $q = d$ in Eqs. (2.10) and (2.11), both of which are dominated by \tilde{r}_3^d and $r_3^d = \tilde{r}_3^d + \tilde{r}_2^d/2$.

3 Amplitude generation

In this section, we highlight some of the technical details of the amplitude generation. Since Γ_{12}^q is computed using the matching coefficients of the $\Delta B = 2$ transition operator, the mixing amplitude is calculated from the $\Delta B = 1$ Hamiltonian as well as the $\Delta B = 2$ transition operator separately. In both cases, we use QGRAF [25] to generate the amplitudes, tapir [26] to generate the topology files and insert Feynman rules, and exp [27, 28] to map the amplitudes to the corresponding topology. The amplitudes are then evaluated using calc, an in-house program written in FORM [29–32] which makes use of color [33] to efficiently evaluate the QCD colour factors. The spinor structures are treated using a projector routine [34], which is integrated into calc and resolves tensor products of two spin lines with up to eleven γ matrices each. In a separate calculation, we use tensor reduction as a cross-check for this step [34]. The resulting scalar integrals are reduced to masters using Kira [35–37], which are then evaluated using the “expand and match” approach [38–41]. For more details on the usage of the individual parts of the toolchain, see Ref. [34].

For the $\Delta B = 2$ transition operator, two-loop diagrams are calculated to obtain the NNLO amplitude, see Fig. 3. The $\Delta B = 2$ side of the matching equation is the same (except for additional evanescent operators) as in Ref. [3] since it does not depend on the type of $\Delta B = 1$ operators used on the other side of the matching. For a more detailed discussion including the $1/m_b$ -suppressed operator R_0 , see Ref. [3].

When calculating the mixing amplitude from two effective $\Delta B = 1$ operators, three-loop

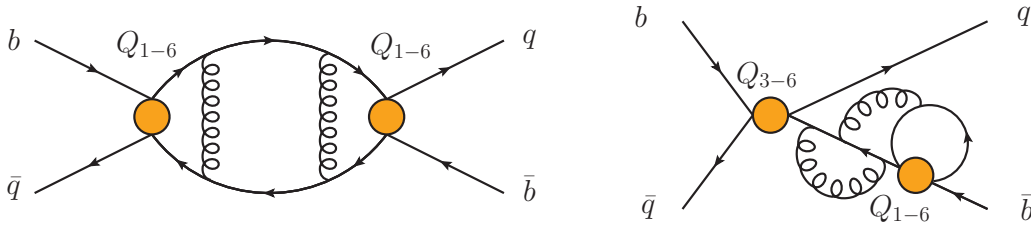


Figure 4: Three-loop Feynman diagrams with two $\Delta B = 1$ insertions shown in orange.

diagrams like the ones shown in Fig. 4 are computed. The diagram type shown on the right is special because it is one-particle reducible with a flavour-changing self-energy (FCSE) on one of the external legs. While the QCD self-energies on external legs can be omitted in the calculation, since the QCD wave function renormalisation cancels from the Wilson coefficients, the corresponding diagrams with an FCSE must be included in the amplitude. These diagrams first appear at NLO when considering insertions of one or more penguin operators.

The calculation of the three-loop amplitudes with up to two penguin operators is challenging from the perspective of the appearing spinor structures. Up to eleven γ matrices appear on each of the two spin lines, requiring the most complicated projectors constructed in Ref. [34]. For the case of one current-current operator and one penguin operator, we have carried out an independent cross-check using tensor integrals and Feynman gauge in the limit of $m_c = 0$. This result depends on nine new three-loop on-shell master integrals (having at most six lines) that were not contained in the set of 23 masters calculated in Ref. [17]. On the level of the unrenormalised three-loop amplitude we found full agreement with the calculation using projectors and an expansion in $z = m_c^2/m_b^2$.

The matching coefficients computed in this work are available in computer-readable format up to z^{10} on the website [42]

4 Phenomenology

In this section, we present our result for the B mixing observables as well as their implications for the determination of the CKM unitarity triangle and new physics searches. The input parameters used in our phenomenological analysis are given in Tab. 1, see also Section 5 of Ref. [3]. In all results presented here, the scale variation is carried out between 2.1 GeV and 8.4 GeV for the purpose of determining the scale uncertainty. This is quoted for the leading and sub-leading $1/m_b$ terms separately in most cases. The uncertainties from the other input parameters are clustered in three groups: the bag parameters B, \tilde{B}_S ; the matrix elements of the $1/m_b$ suppressed operators, and all remaining input variables.

$\alpha_s(M_Z)$	$= 0.1180 \pm 0.0009$	[43]	$\bar{m}_c(3 \text{ GeV})$	$= (0.993 \pm 0.008) \text{ GeV}$	[44]
m_t^{pole}	$= (172.4 \pm 0.7) \text{ GeV}$	[43]	$\bar{m}_b(\bar{m}_b)$	$= (4.163 \pm 0.016) \text{ GeV}$	[45]
M_{B_s}	$= (5366.88 \pm 0.14) \text{ MeV}$	[43]	M_{B_d}	$= (5279.64 \pm 0.12) \text{ MeV}$	[43]
B_{B_s}	$= 0.813 \pm 0.034$	[46]	B_{B_d}	$= 0.806 \pm 0.041$	[46]
\tilde{B}'_{S,B_s}	$= 1.31 \pm 0.09$	[46]	\tilde{B}'_{S,B_d}	$= 1.20 \pm 0.09$	[46]
f_{B_s}	$= (0.2303 \pm 0.0013) \text{ GeV}$	[47–50]	f_{B_d}	$= (0.1905 \pm 0.0013) \text{ GeV}$	[47–50]
ξ	$= (1.216 \pm 0.016)$	[46]	$\frac{f_{B_s}}{f_{B_d}}$	$= (1.2109 \pm 0.0039)$	[47]

Table 1: Input parameters for the numerical analysis. The quoted m_t^{pole} corresponds to $m_t(m_t) = (162.6 \pm 0.7) \text{ GeV}$ in the $\overline{\text{MS}}$ scheme. We use the values for $B_{B_q} = B_{B_q}(\mu_2)$ and $\tilde{B}'_{S,B_q} = \tilde{B}'_{S,B_q}(\mu_2)$ with $\mu_2 = m_b^{\text{pole}}$. For our NNLO results in the pole scheme we convert the quoted $m_b(m_b)$ from the $\overline{\text{MS}}$ scheme with the two-loop formula to $m_b^{\text{pole}} = 4.758 \text{ GeV}$. For the PS scheme predictions we use $m_b^{\text{PS}} = 4.480 \text{ GeV}$ corresponding to a factorisation scale of $\mu_f = 2 \text{ GeV}$. The quoted central values for $m_{c,b}$ imply $\bar{z}(4.2 \text{ GeV}) = (\bar{m}_c(4.2 \text{ GeV})/\bar{m}_b(4.2 \text{ GeV}))^2 = 0.049540$, where the charm mass is calculated for five active quark flavours. The quantity ξ is defined in Eq. (4.15).

4.1 $\Delta\Gamma_q$ and $\Delta\Gamma_q/\Delta M_q$

We start with the quantities $\Delta\Gamma$ and $\Delta\Gamma/\Delta M$ and discuss them separately for the B_s and B_d system. In all cases, we present results in three renormalisation schemes for the overall factor m_b^2 . For our final numerical prediction we choose a combination of the $\overline{\text{MS}}$ and PS scheme. Results for the pole scheme are only provided for comparison.

4.1.1 B_s system

In the three renormalisation schemes our predictions for $\Delta\Gamma_s/\Delta M_s$ are given by

$$\begin{aligned}
\frac{\Delta\Gamma_s}{\Delta M_s} &= \left(3.98_{-0.53\text{scale}}^{+0.49} \quad {}_{-0.19\text{scale}, 1/m_b}^{+0.09} \pm 0.11_{B\tilde{B}_S} \quad \pm 0.78_{1/m_b} \pm 0.06_{\text{input}} \right) \times 10^{-3} \text{ (pole)}, \\
\frac{\Delta\Gamma_s}{\Delta M_s} &= \left(4.45_{-0.40\text{scale}}^{+0.19} \quad {}_{-0.19\text{scale}, 1/m_b}^{+0.09} \pm 0.12_{B\tilde{B}_S} \quad \pm 0.78_{1/m_b} \pm 0.05_{\text{input}} \right) \times 10^{-3} \text{ (\overline{MS})}, \\
\frac{\Delta\Gamma_s}{\Delta M_s} &= \left(4.38_{-0.35\text{scale}}^{+0.33} \quad {}_{-0.19\text{scale}, 1/m_b}^{+0.09} \pm 0.12_{B\tilde{B}_S} \quad \pm 0.78_{1/m_b} \pm 0.05_{\text{input}} \right) \times 10^{-3} \text{ (PS)}, \quad (4.1)
\end{aligned}$$

where the central value is obtained at the scale $\mu_1 = \mu_c = \mu_b = 4.2 \text{ GeV}$.

It is worth noting that the inclusion of the penguin operators up to NNLO results in a reduction of the symmetrised scale uncertainty by about 8% on average compared to Ref. [3]. This is visualised in Fig. 6.

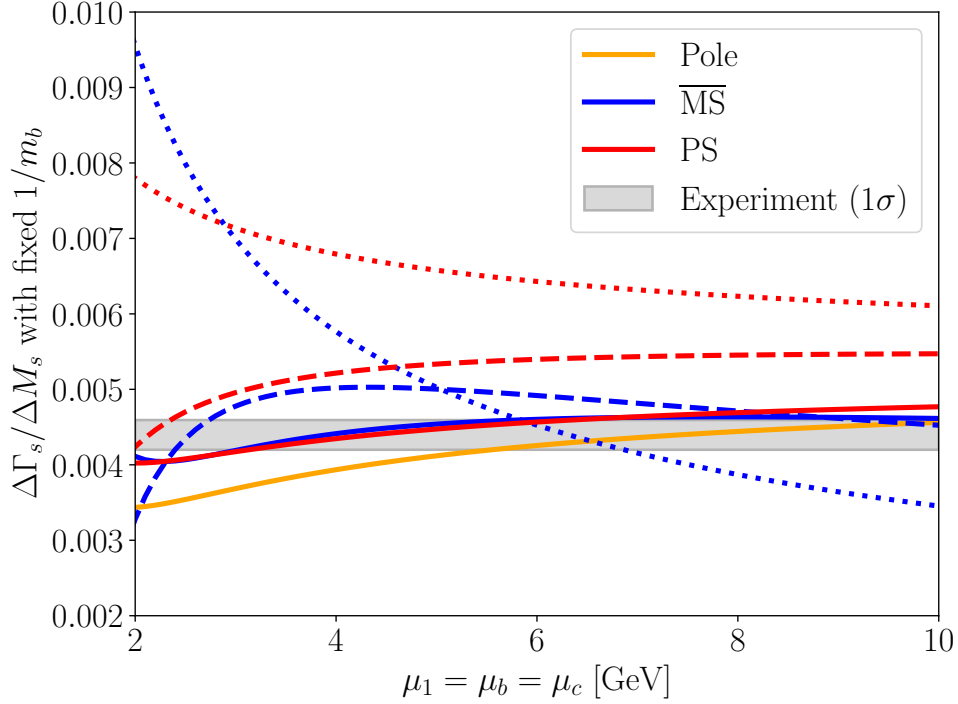


Figure 5: Renormalisation scale dependence at LO (short dashes), NLO (long dashes) and NNLO (solid) for $\Delta\Gamma_s/\Delta M_s$. The plot shows the scale variation of the leading-power terms where the scales $\mu_1 = \mu_b = \mu_c$ are varied together. The grey band shows the experimental value of Eq. (4.5).

The results presented here can be directly compared with Ref. [3] to gauge the impact of a deeper expansion in $z = m_c^2/m_b^2$ at NLO for the penguin contributions as well as the inclusion of the penguin operators at NNLO. For the $\overline{\text{MS}}$ scheme, we note that for the NLO penguin contributions, i.e. those proportional to $C_{1-6} \times C_{3-6}$, the inclusion of all charm mass terms amounts to 30% of the sum of the z^0 and z^1 terms. At NNLO, the penguin operators contribute about 12% to the total NNLO part. As a result, the central value including the $1/m_b$ corrections in the $\overline{\text{MS}}$ and PS schemes is changed by about 2%. Combining the experimental result [51]

$$\Delta M_s^{\text{exp}} = 17.7656 \pm 0.0057 \text{ ps}^{-1} \quad (4.2)$$

with the results in Eq. (4.1) we obtain precise predictions for $\Delta\Gamma_s$:

$$\begin{aligned} \Delta\Gamma_s &= \left(7.06_{-0.94_{\text{scale}}^{+0.88}}^{+0.16} \pm 0.19_{B\tilde{B}_S} \pm 1.39_{1/m_b} \pm 0.10_{\text{input}} \right) \times 10^{-2} \text{ ps}^{-1} \text{ (pole)}, \\ \Delta\Gamma_s &= \left(7.90_{-0.71_{\text{scale}}^{+0.34}}^{+0.16} \pm 0.21_{B\tilde{B}_S} \pm 1.39_{1/m_b} \pm 0.09_{\text{input}} \right) \times 10^{-2} \text{ ps}^{-1} \text{ (\overline{MS})}, \end{aligned}$$

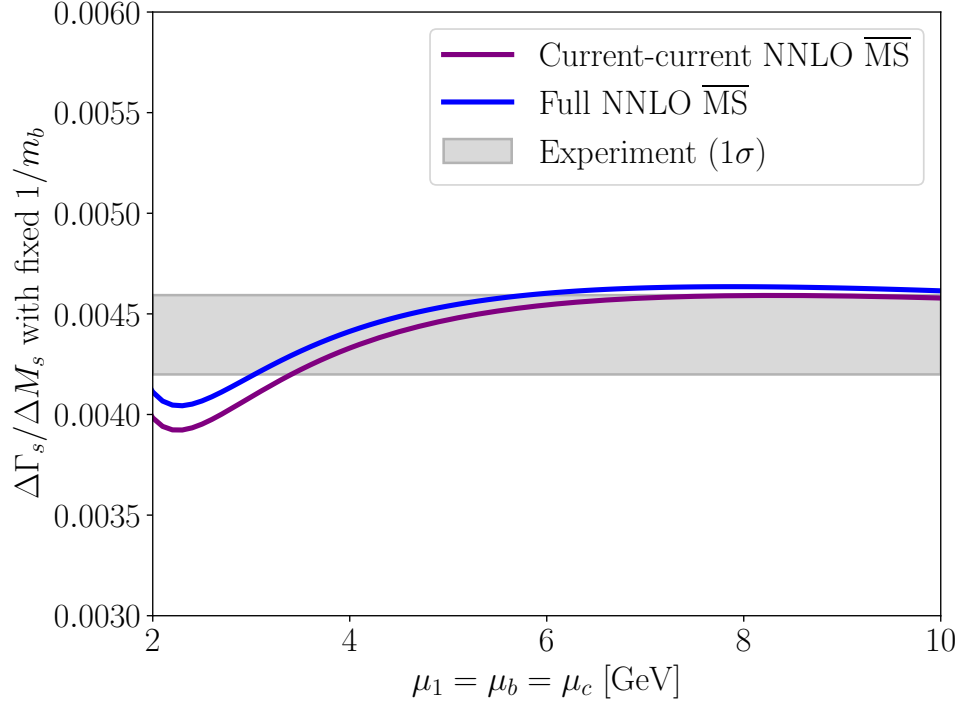


Figure 6: Renormalisation scale dependence in the $\overline{\text{MS}}$ scheme for $\Delta\Gamma_s/\Delta M_s$ with and without penguin operators at NNLO. Note that the current-current result contains a shallow expansion up to z^1 for the NLO penguin contributions whereas the full NNLO result encompasses a deeper expansion up to z^{10} at NLO too. The scale variation shown is of the leading-power terms where the scales $\mu_1 = \mu_b = \mu_c$ are varied together.

$$\Delta\Gamma_s = \left(7.77^{+0.59}_{-0.62} \text{scale}^{+0.16}_{-0.34} \text{scale, } 1/m_b \pm 0.20_{B\tilde{B}_S} \pm 1.39_{1/m_b} \pm 0.09_{\text{input}} \right) \times 10^{-2} \text{ ps}^{-1} \text{ (PS)}. \quad (4.3)$$

The results in the $\overline{\text{MS}}$ and PS schemes are averaged in our final result. For the uncertainty, we add the upper and lower bounds in quadrature, which are then symmetrised and averaged across the schemes. We obtain

$$\Delta\Gamma_s = (0.078 \pm 0.015) \text{ ps}^{-1}, \quad (4.4)$$

which is in excellent agreement with the experimental value [52]

$$\Delta\Gamma_s^{\text{exp}} = (0.0781 \pm 0.0035) \text{ ps}^{-1}, \quad (4.5)$$

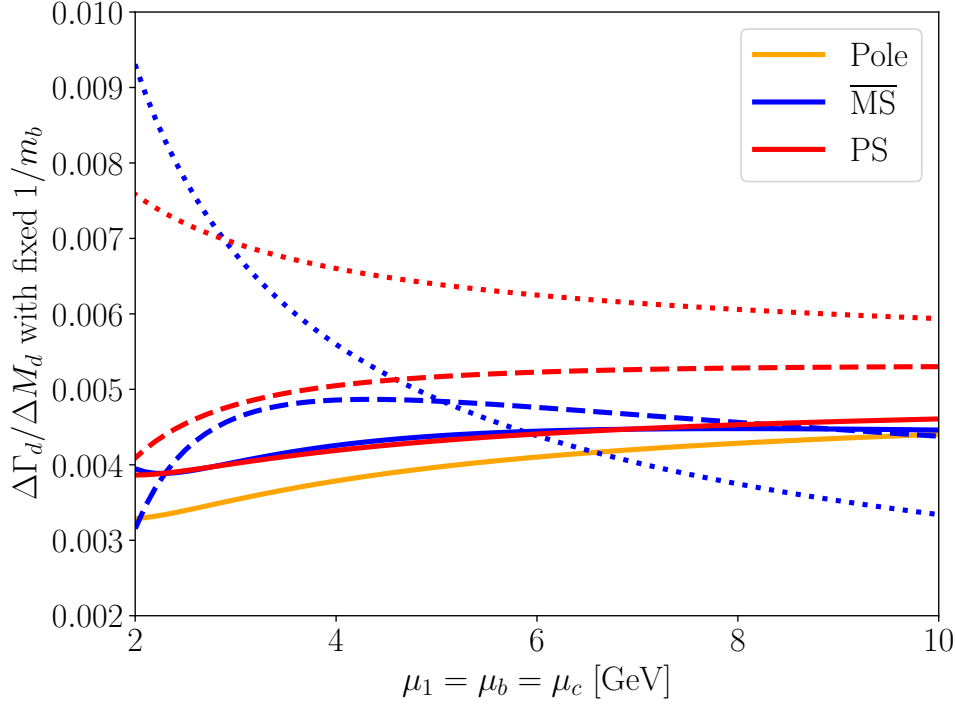


Figure 7: Renormalisation scale dependence at LO (short dashes), NLO (long dashes) and NNLO (solid) for $\Delta\Gamma_d/\Delta M_d$. The scale variation shown is of the leading-power terms where the scales $\mu_1 = \mu_b = \mu_c$ are varied together.

4.1.2 B_d system

In the B_d system, our predictions for $\Delta\Gamma_d/\Delta M_d$ are given by

$$\begin{aligned}
\frac{\Delta\Gamma_d}{\Delta M_d} &= \left(3.83^{+0.49}_{-0.53} \text{scale}^{+0.12}_{-0.20} \text{scale}, 1/m_b \pm 0.11_{B\tilde{B}_S} \pm 0.79_{1/m_b} \pm 0.06_{\text{input}} \right) \times 10^{-3} \text{ (pole)}, \\
\frac{\Delta\Gamma_d}{\Delta M_d} &= \left(4.29^{+0.19}_{-0.40} \text{scale}^{+0.12}_{-0.20} \text{scale}, 1/m_b \pm 0.12_{B\tilde{B}_S} \pm 0.79_{1/m_b} \pm 0.05_{\text{input}} \right) \times 10^{-3} \text{ (}\overline{\text{MS}}\text{)}, \\
\frac{\Delta\Gamma_d}{\Delta M_d} &= \left(4.22^{+0.33}_{-0.35} \text{scale}^{+0.12}_{-0.20} \text{scale}, 1/m_b \pm 0.12_{B\tilde{B}_S} \pm 0.79_{1/m_b} \pm 0.05_{\text{input}} \right) \times 10^{-3} \text{ (PS)}.
\end{aligned}
\tag{4.6}$$

As for the B_s system, we can compare with Ref. [3] to show the impact of our updated calculation with a deeper expansion in $z = m_c^2/m_b^2$ at NLO for the penguin contributions and the penguin operators at NNLO. The NLO penguin contributions including all terms amount to about 26% of the two leading terms in the $\overline{\text{MS}}$ scheme, which is similar to the B_s case. At NNLO, the penguin operators contribute about 12% to the total NNLO part and their inclusion brings down the scale uncertainty of the leading $1/m_b$ terms by almost

10%. The overall result is changed by a similar amount to the B_s system with the central value shifting by about 2%.

In Ref. [12] it was found that at NLO the ratio $\Delta\Gamma_d/\Delta M_d$ receives only small corrections of 2% from the terms proportional to λ_u^d/λ_t^d . i.e. the second and third terms in Eq. (2.4). At NNLO the same behaviour can be observed with the λ_u^d/λ_t^d terms contributing in total only 1.9%. As the ratio $\Delta\Gamma_s/\Delta M_s$ also receives negligible corrections from the terms proportional to the CKM elements, the two ratios have very similar numerical values, see Eqs. (4.1) and (4.6).

Using the experimental value [52]

$$\Delta M_d^{\text{exp}} = (0.5069 \pm 0.0019) \text{ ps}^{-1}, \quad (4.7)$$

we obtain

$$\begin{aligned} \Delta\Gamma_d &= \left(1.94_{-0.27}^{+0.25} \text{scale} \text{ }_{-0.10}^{+0.06} \text{scale, } 1/m_b \pm 0.06_{B\tilde{B}_S} \pm 0.40_{1/m_b} \pm 0.03_{\text{input}} \right) \times 10^{-3} \text{ ps}^{-1} \text{ (pole)}, \\ \Delta\Gamma_d &= \left(2.17_{-0.20}^{+0.10} \text{scale} \text{ }_{-0.10}^{+0.06} \text{scale, } 1/m_b \pm 0.06_{B\tilde{B}_S} \pm 0.40_{1/m_b} \pm 0.03_{\text{input}} \right) \times 10^{-3} \text{ ps}^{-1} \text{ (}\overline{\text{MS}}\text{)}, \\ \Delta\Gamma_d &= \left(2.14_{-0.18}^{+0.17} \text{scale} \text{ }_{-0.10}^{+0.06} \text{scale, } 1/m_b \pm 0.06_{B\tilde{B}_S} \pm 0.40_{1/m_b} \pm 0.03_{\text{input}} \right) \times 10^{-3} \text{ ps}^{-1} \text{ (PS)} \end{aligned} \quad (4.8)$$

from the results in Eq. (4.6) after multiplication with ΔM_d^{exp} . Adding the uncertainties in quadrature for the upper and lower bounds separately, symmetrising the total uncertainty in each scheme and averaging the results for the $\overline{\text{MS}}$ and PS schemes we obtain

$$\Delta\Gamma_d = (0.00215 \pm 0.00045) \text{ ps}^{-1}. \quad (4.9)$$

4.2 a_{fs}^q

From the calculation performed for $\Delta\Gamma_q/\Delta M_q$ we can extract results for a_{fs} by taking the imaginary part of Γ_{12}^q/M_{12}^q . For the B_s system we obtain¹

$$\begin{aligned} a_{\text{fs}}^s &= \left(2.27_{-0.03}^{+0.00} \text{scale} \text{ }_{-0.00}^{+0.01} \text{scale, } 1/m_b \pm 0.01_{B\tilde{B}_S} \pm 0.04_{1/m_b} \pm 0.07_{\text{input}} \right) \times 10^{-5} \text{ (pole)}, \\ a_{\text{fs}}^s &= \left(2.24_{-0.18}^{+0.10} \text{scale} \text{ }_{-0.00}^{+0.01} \text{scale, } 1/m_b \pm 0.01_{B\tilde{B}_S} \pm 0.04_{1/m_b} \pm 0.07_{\text{input}} \right) \times 10^{-5} \text{ (}\overline{\text{MS}}\text{)}, \\ a_{\text{fs}}^s &= \left(2.30_{-0.07}^{+0.03} \text{scale} \text{ }_{-0.00}^{+0.01} \text{scale, } 1/m_b \pm 0.01_{B\tilde{B}_S} \pm 0.04_{1/m_b} \pm 0.07_{\text{input}} \right) \times 10^{-5} \text{ (PS)}. \end{aligned} \quad (4.10)$$

For the B_d system we have²

$$a_{\text{fs}}^d = - \left(5.18_{-0.08}^{+0.00} \text{scale} \text{ }_{-0.01}^{+0.03} \text{scale, } 1/m_b \pm 0.03_{B\tilde{B}_S} \pm 0.09_{1/m_b} \pm 0.16_{\text{input}} \right) \times 10^{-4} \text{ (pole)},$$

¹The uncertainties from the $1/m_b$ bag parameters are smaller than those given in Ref. [3] since the correlation between R_3 , \tilde{R}_3 and \tilde{R}_2 has been accounted for in Eqs. (4.10) and (4.10).

²Note that there is a typo in Eq. (96) of Ref. [3]: The lower limit of the ‘‘scale, $1/m_b$ ’’ uncertainty should read ‘‘ -0.01 ’’ and not ‘‘ -0.08 ’’.

$$\begin{aligned}
a_{\text{fs}}^d &= - \left(5.12_{-0.41}^{+0.23} \text{scale} \text{ }_{-0.01}^{+0.03} \text{scale, } 1/m_b \pm 0.03_{B\tilde{B}_S} \pm 0.09_{1/m_b} \pm 0.16_{\text{input}} \right) \times 10^{-4} \text{ (}\overline{\text{MS}}\text{)}, \\
a_{\text{fs}}^d &= - \left(5.26_{-0.15}^{+0.07} \text{scale} \text{ }_{-0.01}^{+0.03} \text{scale, } 1/m_b \pm 0.03_{B\tilde{B}_S} \pm 0.09_{1/m_b} \pm 0.16_{\text{input}} \right) \times 10^{-4} \text{ (PS)}.
\end{aligned}
\tag{4.11}$$

Comparing our updated results with Ref. [3], we note that the central values of both B_s and B_d are shifted by 0.5% in the $\overline{\text{MS}}$ scheme. In the B_s system, the expansion of the NLO penguin contributions beyond z^1 is as big as this leading term but has the opposite sign. Similarly, both for B_s and B_d the NNLO penguin terms make up about 1% of the NNLO contribution.

Adding the uncertainties in quadrature for the upper and lower bounds, symmetrising the total uncertainty in each scheme, and averaging the results for the $\overline{\text{MS}}$ and PS schemes we obtain

$$\begin{aligned}
a_{\text{fs}}^s &= (2.27 \pm 0.13) \times 10^{-5}, \\
a_{\text{fs}}^d &= -(5.19 \pm 0.30) \times 10^{-4}.
\end{aligned}
\tag{4.12}$$

4.3 The double ratio $(\Delta\Gamma_d/\Delta M_d)/(\Delta\Gamma_s/\Delta M_s)$

The double ratio

$$r_{ds} \equiv \frac{\Delta\Gamma_d}{\Delta M_d} \times \frac{\Delta M_s}{\Delta\Gamma_s}
\tag{4.13}$$

is phenomenologically significant as it can be used to obtain a very accurate prediction for $\Delta\Gamma_d$. This is because the ratio r_{ds} is very close to one, theoretical uncertainties cancel, and the other three quantities, ΔM_d , ΔM_s and $\Delta\Gamma_s$ are measured to high precision.

The ratio happens to be ≈ 1 since most of the dependence on the hadronic matrix elements cancels in Γ_{12}/M_{12} , and additionally the difference stemming from the CKM elements is small. Parametrising the ratio for each of the B_q systems as [12]

$$\frac{\Gamma_{12}^q}{M_{12}^q} = 10^{-4} \left[c^q + a^q \frac{\lambda_u^q}{\lambda_t^q} + b^q \frac{(\lambda_u^q)^2}{(\lambda_t^q)^2} \right],
\tag{4.14}$$

we find that the constants a , b and c only have a weak dependence on the ratio of the hadronic matrix elements $\langle Q \rangle$ and $\langle \tilde{Q}_S \rangle$. In the B_s system, the ratio λ_u^s/λ_t^s is small, and for the B_d system the linear term for $\Delta\Gamma_d/\Delta M_d$ is proportional to $\cos\alpha$, which is close to zero near the apex of the UT (see Fig. 2), while the quadratic correction is doubly Cabibbo-suppressed [12]. As mentioned above, we find that the sum of the a^q and b^q terms contributes about 0.2% and 1.9% for B_s and B_d , respectively.

One additional attractive feature of the double ratio r_{ds} is that the uncertainty of the ratio of the hadronic matrix elements for B_d and B_s is substantially smaller than that of the

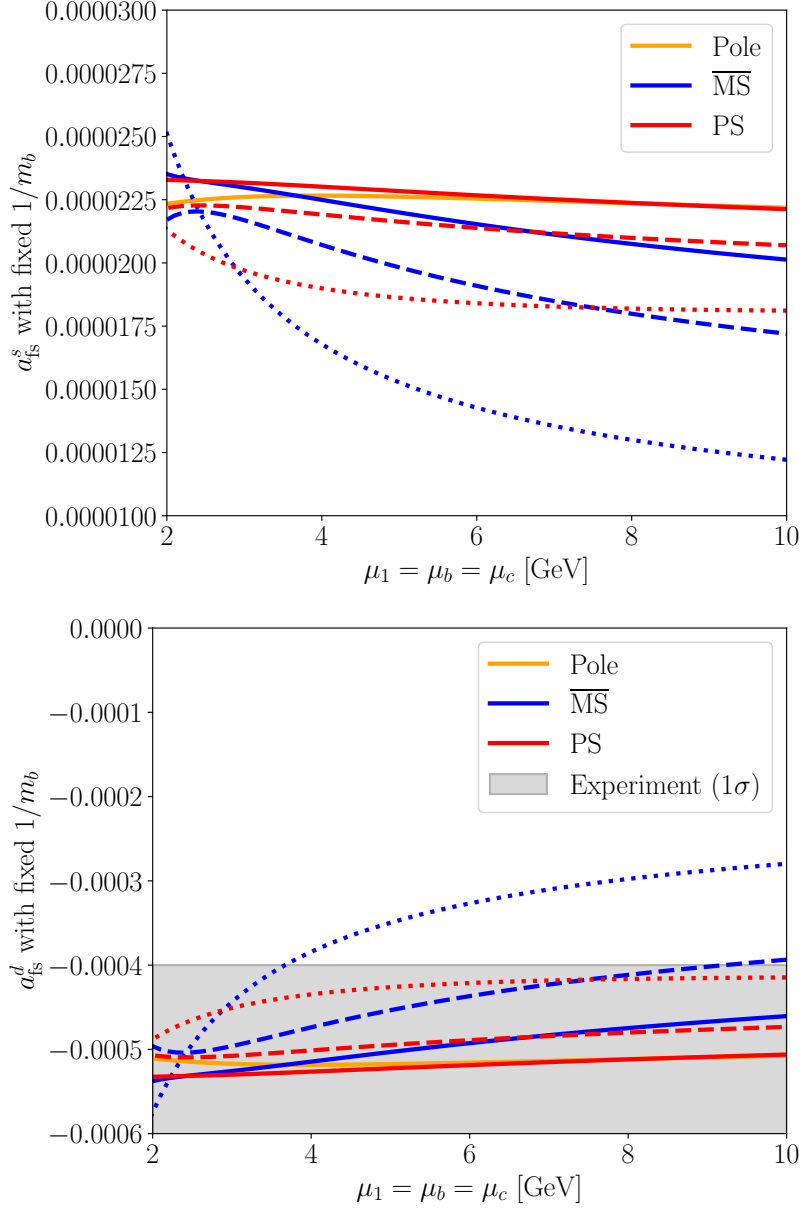


Figure 8: Renormalisation scale dependence at LO (short dashes), NLO (long dashes) and NNLO (solid) for a_{fs}^s (top) and a_{fs}^d (bottom). The scales $\mu_1 = \mu_b = \mu_c$ are varied simultaneously for the leading-power terms while the $1/m_b$ -suppressed terms are kept fixed at the central scale.

individual matrix elements. This feature stems from the fact that the matrix elements are equal in the limit of exact $SU(3)_F$ symmetry. Moreover, the $SU(3)_F$ breaking in the decay constant is precisely known and furthermore $SU(3)_F$ breaking in the bag parameters is found to be small where calculated. Here, we use the parametrisation of the leading order

matrix elements

$$\xi^2 \equiv \frac{f_{B_s}^2 B_{B_s}}{f_{B_d}^2 B_{B_d}}, \quad (4.15)$$

which has been determined very precisely in Ref. [46], see Tab 1. For the bag parameters for $\langle \tilde{Q}_S \rangle$, we calculate a similar ratio

$$\xi_S^2 \equiv \frac{f_{B_s}^2 \tilde{B}'_{S,B_s}}{f_{B_d}^2 \tilde{B}'_{S,B_d}} \quad (4.16)$$

using the numerical value from Ref. [46] (see Tab. XI),

$$\frac{B_{B_s}^{(3)}}{B_{B_d}^{(3)}} = (1.092 \pm 0.034), \quad (4.17)$$

and the ratio of the parameters η_3^s and η_3^d , which we calculate from the definition given in Ref. [46],

$$\frac{\eta_3^s}{\eta_3^d} = (0.996\,51 \pm 0.000\,39). \quad (4.18)$$

For the bag parameters in our convention

$$\tilde{B}'_S \equiv \eta_3 B^{(3)}, \quad (4.19)$$

we combine the results from Eqs. (4.17) and (4.18) to obtain

$$\frac{\tilde{B}'_{S,B_s}}{\tilde{B}'_{S,B_d}} = (1.088 \pm 0.034). \quad (4.20)$$

With the ratio of the decay constants from Tab. 1 we therefore obtain

$$\xi_S = (1.263 \pm 0.020). \quad (4.21)$$

The bag parameters for the $1/m_b$ suppressed matrix elements can also be found in the literature [22, 46]. However, using the results for the B_s and B_d mesons in the double ratio would vastly overestimate the uncertainty. For this reason we proceed as follows: We adopt the values for the bag parameters of the B_s meson from the literature [22, 46]. Afterwards we add manually SU(3)_F-breaking effects. To investigate this effect, we take the numerical values of the bag parameters for B_s mesons obtained from lattice calculations as quoted in Ref. [3] and parametrise the corresponding values in the B_d system using

$$\langle B_q | R_i | \bar{B}_q \rangle \equiv f_{B_q}^2 M_{B_q}^2 B_{R_i, B_q}, \quad B_{R_i, B_d} \equiv \frac{B_{R_i, B_s}}{\zeta}. \quad (4.22)$$

The variable ζ encodes the extent of $SU(3)_F$ symmetry breaking in both the bag parameters. For our numerical analysis we choose

$$\zeta = 1.0 \pm 0.1, \quad (4.23)$$

which allows for up to 10% $SU(3)_F$ breaking. We note that with this parametrisation, only the ratio of the decay constants as given in Tab. 1 is required as numerical input for r_{ds} , not the individual decay constants.

Our results for the double ratio read

$$\begin{aligned} r_{ds} &= 0.9624_{-0.0082_{\text{scale, comb.}}}^{+0.0034} \pm 0.012_{B\tilde{B}_S} \pm 0.040_{1/m_b} \pm 0.003_{\text{input}} \text{ (pole)}, \\ r_{ds} &= 0.9648_{-0.0067_{\text{scale, comb.}}}^{+0.0025} \pm 0.011_{B\tilde{B}_S} \pm 0.036_{1/m_b} \pm 0.003_{\text{input}} \text{ (\overline{MS})}, \\ r_{ds} &= 0.9642_{-0.0058_{\text{scale, comb.}}}^{+0.0025} \pm 0.012_{B\tilde{B}_S} \pm 0.036_{1/m_b} \pm 0.003_{\text{input}} \text{ (PS)}. \end{aligned} \quad (4.24)$$

Note that the uncertainty of the $1/m_b$ -suppressed terms stems mainly from the unknown size of $SU(3)_F$ breaking. Neglecting the uncertainty of ζ , the uncertainty labelled $1/m_b$ is just ± 0.008 . In Fig. 9 we show the remaining renormalisation scale dependence of the leading and sub-leading $1/m_b$ terms combined of the double ratio. It is worth commenting on the increasing scale dependence from LO to NNLO. This is due to the fact that the scale dependence of the Γ_{12}/M_{12} ratios in the B_s and B_d systems are almost identical, see Figs. 5 and 7. Therefore, small deviations which appear at higher orders lead to a seemingly worse convergence of the perturbative series. However, overall the scale dependence of the leading power terms is still small and the prediction of r_{ds} very accurate.

Averaging the results of the $\overline{\text{MS}}$ and PS schemes and adding the uncertainties of the upper and lower bounds in quadrature before symmetrising, we obtain our final result for the double ratio

$$r_{ds} = 0.965 \pm 0.038. \quad (4.25)$$

Using this together with the experimental values of the mass differences from Eq. (4.7) and Eq. (4.2) as well as $\Delta\Gamma_s$ from Eq. (4.5) we obtain our most accurate theoretical prediction of

$$\Delta\Gamma_d = (0.00215 \pm 0.00013) \text{ ps}^{-1}. \quad (4.26)$$

Comparing this result to the previously obtained value in Eq. (4.9), the uncertainty has been reduced by 70% thanks to the better control of the hadronic uncertainties in the double ratio r_{ds} .

4.4 Unitarity triangle constraints from a_{fs}^d and $\Delta\Gamma_d/\Delta\Gamma_s$

As shown in Fig. 2, future measurements of a_{fs}^d and $\Delta\Gamma_d$ will lead to important constraints on the apex $(\bar{\rho}, \bar{\eta})$ of the unitarity triangle.

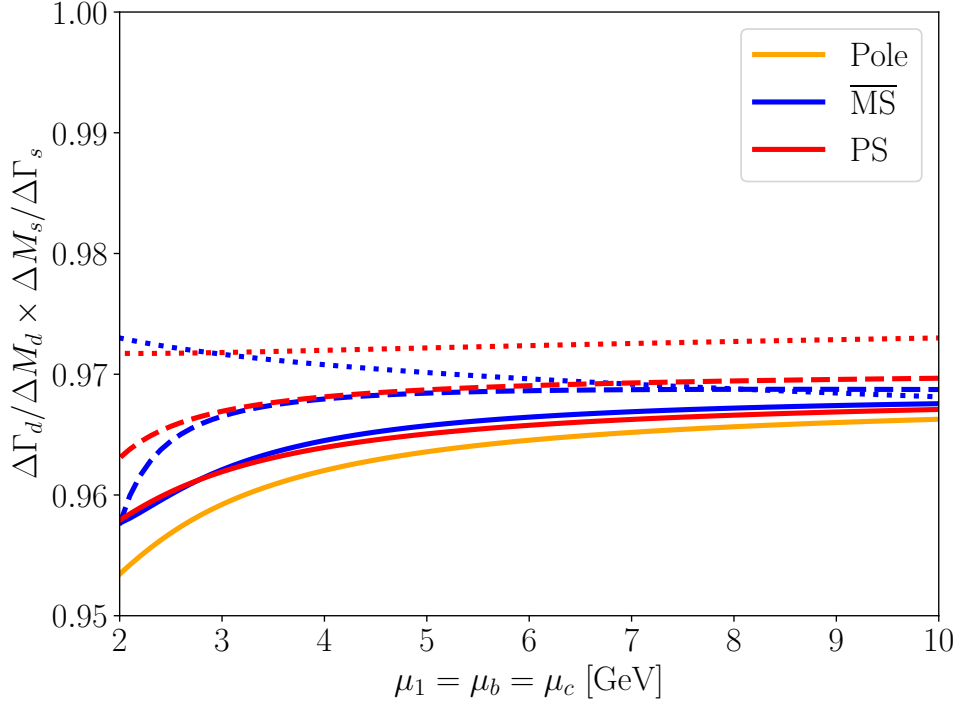


Figure 9: Renormalisation scale dependence at LO (short dashes), NLO (long dashes) and NNLO (solid) for r_{ds} . The scale variation shown is of the leading and sub-leading terms in the HQE where the scales $\mu_1 = \mu_b = \mu_c$ are varied together. Note that for the NLO and NNLO scale dependence, the respective α_s corrections were included in the individual Γ_{12}/M_{12} ratios without truncating the double ratio in α_s .

We update the constraint from a_{fs}^d shown in Fig. 8 of Ref. [3] and further discuss the ratio $\Delta\Gamma_d/\Delta\Gamma_s$, from which many of the theoretical uncertainties cancel. For these analyses, it is useful to define the quantities a , b , and c via Eq. (4.14). With Eq. (2.4) one finds

$$\begin{aligned}
c^q &= -10^4 \frac{(\lambda_t^q)^2}{M_{12}^q} \Gamma_{12}^{cc}, \\
a^q &= -2 \cdot 10^4 \frac{(\lambda_t^q)^2}{M_{12}^q} (\Gamma_{12}^{cc} - \Gamma_{12}^{uc}), \\
b^q &= -10^4 \frac{(\lambda_t^q)^2}{M_{12}^q} (\Gamma_{12}^{uu} + \Gamma_{12}^{cc} - 2\Gamma_{12}^{uc}),
\end{aligned} \tag{4.27}$$

which is convenient because $(\lambda_t^q)^2/M_{12}^q$ and thus a , b , and c are real, and the ratios λ_u^q/λ_t^q in Eq. (4.14) have simple expressions in terms of the improved Wolfenstein parameters. For $q = d$ the latter are given in Eq. (1.13) and for $q = s$ we have

$$\frac{\lambda_u^s}{\lambda_t^s} = \lambda^2(-\bar{\rho} + i\bar{\eta}) + \lambda^4(-\bar{\rho}(1 - \bar{\rho}) - \bar{\eta}^2 + i\bar{\eta}(1 - 2\bar{\rho})) + \mathcal{O}(\lambda^6), \tag{4.28}$$

where $\lambda \simeq |V_{us}|$ with $\lambda = 0.225$ is a Wolfenstein parameter.

The ratio of the width differences can be written as

$$\frac{\Delta\Gamma_d}{\Delta\Gamma_s} = \frac{1}{\xi^2} \frac{M_{B_d}}{M_{B_s}} \left| \frac{\lambda_t^d}{\lambda_t^s} \right|^2 \frac{c^d + a^d \operatorname{Re} \frac{\lambda_u^d}{\lambda_t^d} + b^d \operatorname{Re} \frac{(\lambda_u^d)^2}{(\lambda_t^d)^2}}{c^s + a^s \operatorname{Re} \frac{\lambda_u^s}{\lambda_t^s} + b^s \operatorname{Re} \frac{(\lambda_u^s)^2}{(\lambda_t^s)^2}}, \quad (4.29)$$

where the ratio ξ^2 from Eq. (4.15) was used. For Eq. (4.29) we need a further parametrisation of the CKM factors in terms of $\bar{\rho}$ and $\bar{\eta}$,

$$\left| \frac{\lambda_t^d}{\lambda_t^s} \right|^2 = \lambda^2 (\bar{\eta}^2 + (1 - \bar{\rho})^2) \times (1 + \lambda^2(1 - 2\bar{\rho})) + \mathcal{O}(\lambda^6). \quad (4.30)$$

The ratio in Eq. (4.29) can be further simplified since the numerical values of $\{a^d, b^d, c^d\}$ and $\{a^s, b^s, c^s\}$ agree very well within their (perturbative) uncertainties, see Tabs. 2 and 3. We can thus simplify the ratio in Eq. (4.29) to

$$\frac{\Delta\Gamma_d}{\Delta\Gamma_s} = \frac{1}{\xi^2} \frac{M_{B_d}}{M_{B_s}} \left| \frac{\lambda_t^d}{\lambda_t^s} \right|^2 \frac{1 + \frac{a}{c} \operatorname{Re} \frac{\lambda_u^d}{\lambda_t^d} + \frac{b}{c} \operatorname{Re} \frac{(\lambda_u^d)^2}{(\lambda_t^d)^2}}{1 + \frac{a}{c} \operatorname{Re} \frac{\lambda_u^s}{\lambda_t^s} + \frac{b}{c} \operatorname{Re} \frac{(\lambda_u^s)^2}{(\lambda_t^s)^2}}, \quad (4.31)$$

where the superscripts were dropped.

The flavour-specific CP asymmetry a_{fs}^d is similarly parametrised as

$$a_{\text{fs}}^d = \left[a \operatorname{Im} \frac{\lambda_u^d}{\lambda_t^d} + b \operatorname{Im} \frac{(\lambda_u^d)^2}{(\lambda_t^d)^2} \right] \times 10^{-4}. \quad (4.32)$$

By inserting Eqs. (1.13) and (4.28) into Eq. (4.31) one finds the constraint on $(\bar{\rho}, \bar{\eta})$ defined by $\Delta\Gamma_d/\Delta\Gamma_s$. Analogously the constraint from a_{fs}^d is obtained by inserting Eq. (1.13) into Eq. (4.32).

In order to construct the constraints on the CKM triangle, we calculate the quantities a , b and c in Eq. (4.14) to LO, NLO and NNLO. These constants can be further decomposed into a leading and sub-leading $1/m_b$ -suppressed contribution,

$$\begin{aligned} a &= a_0 + a_1, \\ b &= b_0 + b_1, \\ c &= c_0 + c_1, \end{aligned} \quad (4.33)$$

where the subscripts 0 and 1 denote the leading and sub-leading terms of the HQE respectively. The sub-leading contributions of a^d and b^d have been calculated previously

$\overline{\text{MS}}$	LO	NLO	NNLO	PS	LO	NLO	NNLO
a_0^d	$8.20^{+4.20}_{-1.94}$	$10.40^{+0.81}_{-1.45}$	$11.40^{+0.55}_{-0.95}$	a_0^d	$9.53^{+1.17}_{-0.39}$	$11.11^{+0.22}_{-0.50}$	$11.71^{+0.15}_{-0.35}$
b_0^d	$0.069^{+0.037}_{-0.020}$	$0.112^{+0.043}_{-0.020}$	$0.134^{+0.042}_{-0.022}$	b_0^d	$0.081^{+0.011}_{-0.009}$	$0.122^{+0.027}_{-0.008}$	$0.140^{+0.034}_{-0.015}$
c_0^d	$-69.7^{+17.7}_{-35.0}$	$-64.1^{+14.2}_{-0.0}$	$-58.3^{+4.0}_{-1.9}$	c_0^d	$-81.0^{+5.2}_{-9.4}$	$-66.2^{+8.7}_{-2.1}$	$-57.6^{+3.5}_{-3.3}$

Table 2: Updated results for the values a_0^d , b_0^d and c_0^d in the $\overline{\text{MS}}$ (left) and PS (right) schemes for the B_d system. The uncertainty shown here is the perturbative scale uncertainty obtained from varying $\mu_1 = \mu_b = \mu_c$ simultaneously between 2.1 GeV and 8.4 GeV.

and are given in Ref. [3]. For completeness we list them again here together with the new value for c ,

$$\begin{aligned}
a_1^d &= 0.622^{+0.073}_{-0.020_{\text{scale}}} \pm 0.35_{\text{para}} , \\
b_1^d &= 0.091^{+0.011}_{-0.003_{\text{scale}}} \pm 0.031_{\text{para}} , \\
c_1^d &= 15.36^{+1.98}_{-1.22_{\text{scale}}} \pm 8.03_{\text{para}} ,
\end{aligned} \tag{4.34}$$

where the uncertainties from varying all input parameters have been attributed to the sub-leading terms, denoted “para”. The leading contributions a_0, b_0, c_0 hence only have a scale uncertainty. The “para” uncertainty is dominated by m_c for a_1 and b_1 while \tilde{r}_2^q has the biggest impact for c_1 . Note that the scale uncertainties are obtained as before by varying $\mu_1 = \mu_b = \mu_c$ simultaneously between 2.1 GeV and 8.4 GeV. The sub-leading term is only known to LO and is therefore the same for all renormalisation schemes up to minor differences in the parametric uncertainties. For the B_s system we find similarly

$$\begin{aligned}
a_1^s &= 0.616^{+0.074}_{-0.025_{\text{scale}}} \pm 0.35_{\text{para}} , \\
b_1^s &= 0.090^{+0.011}_{-0.004_{\text{scale}}} \pm 0.030_{\text{para}} , \\
c_1^s &= 15.28^{+1.90}_{-0.93_{\text{scale}}} \pm 7.90_{\text{para}} ,
\end{aligned} \tag{4.35}$$

For the leading- $1/m_b$ contributions, the results in the $\overline{\text{MS}}$ and PS schemes are given in Tab. 2. When comparing to the results obtained for the current-current contributions only at NNLO in Ref. [3], we note that b_0 is unchanged because the penguin operators do not yield additional contributions to the $(\lambda_u^d)^2$ term. In fact, only the mixed current-current penguin contributions affect a_{fs} , and only in terms of a_0 . The results for c_0 are entirely new.

Using the numerical values of a , b and c given here, the constraints shown in Fig. 10 can be plotted, where the error bands only include the uncertainty from the scale variation of the leading- $1/m_b$ term. To motivate more accurate determinations of the quantities a_{fs}^d and $\Delta\Gamma_d$, we have shown the constraints stemming from hypothetical measurements

$\overline{\text{MS}}$	LO	NLO	NNLO	PS	LO	NLO	NNLO
a_0^s	$8.23^{+4.21}_{-1.94}$	$10.43^{+0.82}_{-1.46}$	$11.44^{+0.56}_{-0.96}$	a_0^s	$9.56^{+1.17}_{-0.39}$	$11.15^{+0.23}_{-0.50}$	$11.76^{+0.16}_{-0.35}$
b_0^s	$0.072^{+0.038}_{-0.021}$	$0.115^{+0.043}_{-0.021}$	$0.137^{+0.042}_{-0.022}$	b_0^s	$0.083^{+0.011}_{-0.009}$	$0.125^{+0.026}_{-0.007}$	$0.143^{+0.034}_{-0.015}$
c_0^s	$-71.1^{+18.2}_{-35.8}$	$-65.4^{+14.5}_{-0.0}$	$-59.6^{+3.9}_{-1.9}$	c_0^s	$-82.6^{+5.4}_{-9.6}$	$-67.6^{+8.9}_{-2.1}$	$-58.9^{+3.5}_{-3.3}$

Table 3: Updated results for the values a_0^s , b_0^s and c_0^s in the $\overline{\text{MS}}$ (left) and PS (right) schemes for the B_s system. The uncertainty shown here is the perturbative scale uncertainty obtained from varying $\mu_1 = \mu_b = \mu_c$ simultaneously between 2.1 GeV and 8.4 GeV.

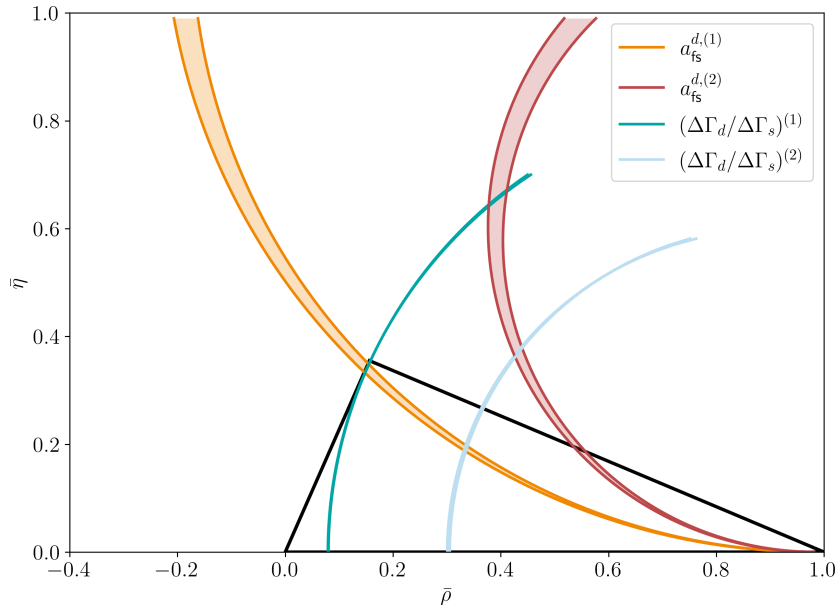


Figure 10: Constraints on the apex of the CKM triangle in the PS scheme. The bands correspond to the perturbative uncertainty of the leading- $1/m_b$ term, which have been added in quadrature, and are plotted for $a_{\text{fs}}^{d,(1)} = -5 \times 10^{-4}$, $a_{\text{fs}}^{d,(2)} = -1 \times 10^{-3}$, $(\Delta\Gamma_d/\Delta\Gamma_s)^{(1)} = 0.029$ and $(\Delta\Gamma_d/\Delta\Gamma_s)^{(2)} = 0.0145$.

differing by a factor of two. Since all terms involving a/c or b/c are small, $\Delta\Gamma_d/\Delta\Gamma_s$ can be predicted with high precision. The factor $|\lambda_t^d|^2/|\lambda_t^s|^2$ is the same as in $\Delta M_d/\Delta M_s$, so that the curve in the $(\bar{\rho}, \bar{\eta})$ plane looks very similar to the corresponding circle around $(1, 0)$ with radius R_t shown in light red in Fig. 2. Since $\Delta\Gamma_d/\Delta\Gamma_s$ and $\Delta M_d/\Delta M_s$ depend on new-physics parameters in a very different way, this feature can be used to identify new physics in either ratio or in other quantities entering the global fit of $(\bar{\rho}, \bar{\eta})$.

To illustrate the size of the uncertainties of all input parameters, including the non-perturbative matrix elements, compared with the perturbative uncertainties of our calcu-

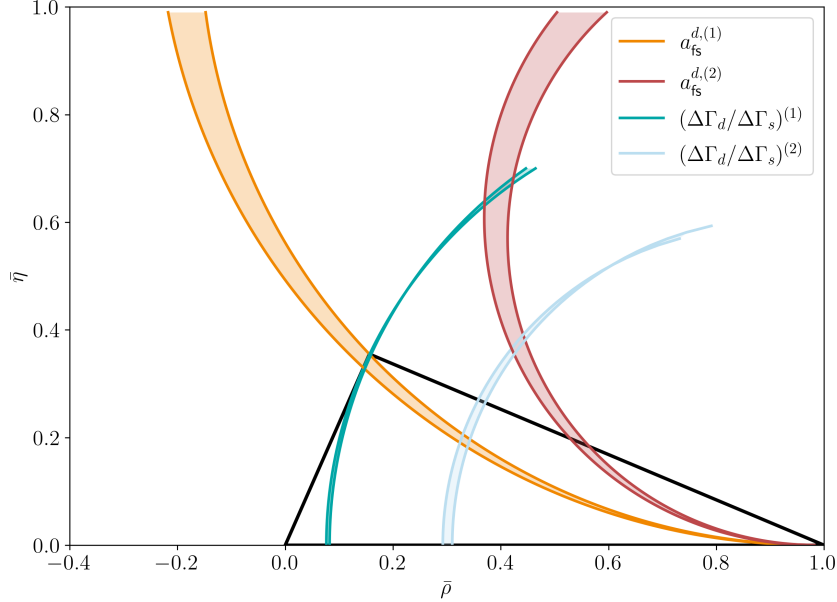


Figure 11: Constraints on the apex of the CKM triangle in the PS scheme. The bands correspond to the full uncertainty and are plotted for $a_{\text{fs}}^{d,(1)} = -5 \times 10^{-4}$, $a_{\text{fs}}^{d,(2)} = -1 \times 10^{-3}$, $(\Delta\Gamma_d/\Delta\Gamma_s)^{(1)} = 0.029$ and $(\Delta\Gamma_d/\Delta\Gamma_s)^{(2)} = 0.0145$. The perturbative uncertainties of the leading-power and $1/m_b$ -suppressed contributions have been added in quadrature here.

lations, we also show the constraints on the apex of the CKM triangle with all uncertainties combined in Fig. 11. We observe that the bands for $\Delta\Gamma_d/\Delta\Gamma_s$ are still very narrow and the current status of theoretical predictions lead to strong constraints on the apex of the unitarity triangle. This is possible because the ratio of the leading- $1/m_b$ matrix elements is proportional to ξ^2 , which has been determined very accurately on the lattice.

4.5 Numerical results independent of CKM values and hadronic matrix elements

In this section, we present our results independent of any input values pertaining to the CKM matrix or the hadronic matrix elements, which carry most of the input uncertainties. Following Eq. (4.14), we write

$$\frac{\Gamma_{12}^q}{M_{12}^q} = 10^{-4} \times \sum_O \left[c_O + a_O \frac{\lambda_u^q}{\lambda_t^q} + b_O \frac{\lambda_u^{q2}}{\lambda_t^{q2}} \right] \frac{\langle B_q | O | \bar{B}_q \rangle}{\langle B_q | Q | \bar{B}_q \rangle}, \quad (4.36)$$

where the sum is over the set of operators

$$O \in \{Q, \tilde{Q}_S, R_0, R_1, \tilde{R}_1, \tilde{R}_2, \tilde{R}_3\}. \quad (4.37)$$

$\overline{\text{MS}}$	c_O	a_O	b_O
Q	$-42.6^{+4.4}_{-1.8} \pm 0.5$	$10.9^{+0.46}_{-0.90} \pm 0.21$	$0.108^{+0.038}_{-0.023} \pm 0.005$
\tilde{Q}_S	$-84.6^{+0.88}_{-2.90} \pm 0.99$	$2.66^{+0.48}_{-0.28} \pm 0.11$	$0.141^{+0.023}_{-0.000} \pm 0.011$

Table 4: Results in the $\overline{\text{MS}}$ scheme for the individual matrix element coefficients with the two-sided perturbative and symmetrised input uncertainty. The scale uncertainty is obtained from varying $\mu_1 = \mu_b = \mu_c$ simultaneously between 2.1 GeV and 8.4 GeV.

PS	c_O	a_O	b_O
Q	$-41.9^{+3.7}_{-2.7} \pm 0.5$	$11.20^{+0.08}_{-0.32} \pm 0.23$	$0.115^{+0.030}_{-0.017} \pm 0.006$
\tilde{Q}_S	$-84.4^{+0.8}_{-3.0} \pm 1.0$	$2.74^{+0.39}_{-0.16} \pm 0.11$	$0.139^{+0.022}_{-0.000} \pm 0.012$

Table 5: Results in the PS scheme for the individual matrix element coefficients with the two-sided perturbative and symmetrised input uncertainty. The scale uncertainty is obtained from varying $\mu_1 = \mu_b = \mu_c$ simultaneously between 2.1 GeV and 8.4 GeV.

Note that the matrix elements of R_2 and R_3 were eliminated using [20]

$$\begin{aligned}
R_2 &= -\tilde{R}_2, \\
R_3 &= \tilde{R}_3 + \frac{1}{2}\tilde{R}_2,
\end{aligned}
\tag{4.38}$$

which holds up to corrections of higher order in α_s and $1/m_b$. In the parametrisation of Eq. (4.36), all input parameters that depend on the specific B_q mesons was factored out such that the constants a_O , b_O and c_O are the same for B_s and B_d . The results are given in Tabs. 4, 5 and 6, where the $1/m_b$ -suppressed terms do not differ between the two schemes since they are only known to LO. The uncertainties of all coefficients are dominated by the scale uncertainty since the remaining input parameters have a minor impact on the final result and are known relatively precisely.

The values given in Tabs. 4, 5 and 6 can be used to update, e.g. the constraints on the CKM triangle as shown in Fig. 11 once more accurate results for input values like the hadronic matrix elements become available. It is worth noting that the constraints from $\Delta\Gamma_d/\Delta\Gamma_s$ are essentially unchanged with the current input values whether the simplified formula from Eq. (4.31) or the full parametrisation in Eq. (4.36) is used.

5 Conclusions

In this paper, we complete the NNLO corrections from leading-power operators to the decay width difference and the charge-parity asymmetry. We include all current-current

$1/m_b$	$c_{\mathcal{O}}$	$a_{\mathcal{O}}$	$b_{\mathcal{O}}$
R_0	$27.9_{-5.2}^{+4.3} \pm 0.5$	$-0.493_{-0.076}^{+0.093} \pm 0.019$	$-0.0449_{-0.0069}^{+0.0084} \pm 0.0024$
R_1	$-55.8_{-8.6}^{+10.5} \pm 0.9$	$0.99_{-0.19}^{+0.15} \pm 0.04$	$0.090_{-0.017}^{+0.014} \pm 0.005$
\tilde{R}_1	$172_{-14}^{+22} \pm 2$	$-3.05_{-0.39}^{+0.25} \pm 0.11$	$-0.277_{-0.036}^{+0.023} \pm 0.015$
\tilde{R}_2	$231_{-25}^{+31} \pm 3$	$-0.73_{-0.12}^{+0.16} \pm 0.02$	$0.0615_{-0.0000}^{+0.0058} \pm 0.0036$
\tilde{R}_3	$3.89_{-0.12}^{+0.46} \pm 0.14$	$4.47_{-0.14}^{+0.53} \pm 0.17$	$0.579_{-0.018}^{+0.068} \pm 0.032$

Table 6: Results for the $1/m_b$ -suppressed matrix element coefficients with the two-sided perturbative and symmetrised input uncertainty. The scale uncertainty is obtained from varying $\mu_1 = \mu_b = \mu_c$ simultaneously between 2.1 GeV and 8.4 GeV.

and penguin operators in the three-loop contributions of the $|\Delta B| = 1$ part and incorporate the full charm quark mass dependence through deep expansions in m_c/m_b . New ingredients from this paper are the penguin contributions at NNLO and their full charm quark mass dependence at NLO.

We perform a detailed phenomenological analysis of $\Delta\Gamma_q$ and a_{fs}^q both for the B_s and the B_d system. The inclusion of the penguin contribution at NNLO leads to shifts below 2% and 0.5% for $\Delta\Gamma_q$ and a_{fs}^q respectively for the central values of the renormalisation scale. However, we observe a further stabilisation of the dependence on the renormalisation scale which we use to estimate the uncertainties from unknown higher-order corrections. They amount to about $\pm 7\%$ for $\Delta\Gamma_q$ and $\pm 5\%$ for a_{fs}^q . A further reduction requires a four-loop calculation in the $|\Delta B| = 1$ theory accompanied by a three-loop calculation on the $|\Delta B| = 2$ side together with a proper definition of the corresponding evanescent operators. Such a calculation will most likely not be available in the foreseeable future.

In our prediction the dominant uncertainty stems from $1/m_b$ corrections. In order to allow for a simple incorporation of future improvements, we provide ready-to-use formulae for $\Delta\Gamma_q/\Delta M_q$ where updated values for the leading and $1/m_b$ -suppressed bag parameters can be inserted in a straightforward way.

A phenomenological interesting quantity is the double ratio $(\Delta\Gamma_s/\Delta M_s)/(\Delta\Gamma_d/\Delta M_d)$ since hadronic uncertainties cancel to a large extent, and the perturbative uncertainty is reduced to the sub-percent level. We calculate the most accurate prediction of $\Delta\Gamma_d$ to date with a combined uncertainty of around 6%, which can be further reduced to the sub-percent level with more accurate determinations of the hadronic bag parameters.

Finally, we combine the predictions for a_{fs}^d and $\Delta\Gamma_d/\Delta\Gamma_s$ to show how the apex of the CKM triangle can be constrained from mixing observables in the B_d and B_s system alone, without the information from a global fit to CKM parameters. We find that the constraints

from a_{fs}^d and in particular $\Delta\Gamma_d/\Delta\Gamma_s$ yield very stringent constraints given a particular set of measurements, which motivates more accurate experimental determinations of the B mixing observables.

Acknowledgements

The work was supported by the Deutsche Forschungsgemeinschaft (DFG, German Research Foundation) under grant 396021762 — TRR 257 “Particle Physics Phenomenology after the Higgs Discovery”. Pascal Reeck would like to thank the Studienstiftung des deutschen Volkes for supporting him.

References

- [1] A.J. Buras, W. Slominski and H. Steger, $B^0 - \bar{B}^0$ Mixing, CP Violation and the B Meson Decay, *Nucl. Phys. B* **245** (1984) 369.
- [2] U. Nierste, *CP asymmetry in flavor-specific B decays*, in *Proceedings of 39th Rencontres de Moriond on Electroweak Interactions and Unified Theories*, pp. 445–450, 6, 2004 [[hep-ph/0406300](#)].
- [3] M. Gerlach, U. Nierste, P. Reeck, V. Shtabovenko and M. Steinhauser, *Current-current operator contribution to the decay matrix in B-meson mixing at next-to-next-to-leading order of QCD*, [2505.22740](#).
- [4] G. Alonso-Álvarez, G. Elor and M. Escudero, *Collider signals of baryogenesis and dark matter from B mesons: A roadmap to discovery*, *Phys. Rev. D* **104** (2021) 035028 [[2101.02706](#)].
- [5] V.A. Khoze, M.A. Shifman, N.G. Uraltsev and M.B. Voloshin, *On Inclusive Hadronic Widths of Beautiful Particles*, *Sov. J. Nucl. Phys.* **46** (1987) 112.
- [6] A.J. Buras and P.H. Weisz, *QCD Nonleading Corrections to Weak Decays in Dimensional Regularization and 't Hooft-Veltman Schemes*, *Nucl. Phys. B* **333** (1990) 66.
- [7] A.J. Buras, M. Jamin, M.E. Lautenbacher and P.H. Weisz, *Effective Hamiltonians for $\Delta S = 1$ and $\Delta B = 1$ nonleptonic decays beyond the leading logarithmic approximation*, *Nucl. Phys. B* **370** (1992) 69.
- [8] M. Gorbahn and U. Haisch, *Effective Hamiltonian for non-leptonic $|\Delta F| = 1$ decays at NNLO in QCD*, *Nucl. Phys. B* **713** (2005) 291 [[hep-ph/0411071](#)].
- [9] M. Misiak and M. Munz, *Two loop mixing of dimension five flavor changing operators*, *Phys. Lett. B* **344** (1995) 308 [[hep-ph/9409454](#)].
- [10] K.G. Chetyrkin, M. Misiak and M. Munz, *Weak radiative B meson decay beyond leading logarithms*, *Phys. Lett. B* **400** (1997) 206 [[hep-ph/9612313](#)].

- [11] M. Beneke, G. Buchalla, C. Greub, A. Lenz and U. Nierste, *Next-to-leading order QCD corrections to the lifetime difference of B_s mesons*, *Phys. Lett. B* **459** (1999) 631 [[hep-ph/9808385](#)].
- [12] M. Beneke, G. Buchalla, A. Lenz and U. Nierste, *CP Asymmetry in Flavor Specific B Decays beyond Leading Logarithms*, *Phys. Lett. B* **576** (2003) 173 [[hep-ph/0307344](#)].
- [13] A. Lenz and U. Nierste, *Theoretical update of $B_s - \bar{B}_s$ mixing*, *JHEP* **06** (2007) 072 [[hep-ph/0612167](#)].
- [14] H.M. Asatrian, A. Hovhannisyanyan, U. Nierste and A. Yeghiazaryan, *Towards next-to-next-to-leading-log accuracy for the width difference in the $B_s - \bar{B}_s$ system: fermionic contributions to order $(m_c/m_b)^0$ and $(m_c/m_b)^1$* , *JHEP* **10** (2017) 191 [[1709.02160](#)].
- [15] H.M. Asatrian, H.H. Asatryan, A. Hovhannisyanyan, U. Nierste, S. Tumasyan and A. Yeghiazaryan, *Penguin contribution to the width difference and CP asymmetry in $B_q - \bar{B}_q$ mixing at order $\alpha_s^2 N_f$* , *Phys. Rev. D* **102** (2020) 033007 [[2006.13227](#)].
- [16] A. Hovhannisyanyan and U. Nierste, *Addendum to: Towards next-to-next-to-leading-log accuracy for the width difference in the $B_s - \bar{B}_s$ system: fermionic contributions to order $(m_c/m_b)^0$ and $(m_c/m_b)^1$* , *JHEP* **06** (2022) 090 [[2204.11907](#)].
- [17] M. Gerlach, U. Nierste, V. Shtabovenko and M. Steinhauser, *Width Difference in the $B - \bar{B}$ System at Next-to-Next-to-Leading Order of QCD*, *Phys. Rev. Lett.* **129** (2022) 102001 [[2205.07907](#)].
- [18] M. Gerlach, U. Nierste, V. Shtabovenko and M. Steinhauser, *Two-loop QCD penguin contribution to the width difference in $B_s - \bar{B}_s$ mixing*, *JHEP* **07** (2021) 043 [[2106.05979](#)].
- [19] M. Gerlach, U. Nierste, V. Shtabovenko and M. Steinhauser, *The width difference in $B - \bar{B}$ mixing at order α_s and beyond*, *JHEP* **04** (2022) 006 [[2202.12305](#)].
- [20] M. Beneke, G. Buchalla and I. Dunietz, *Width Difference in the $B_s - \bar{B}_s$ System*, *Phys. Rev. D* **54** (1996) 4419 [[hep-ph/9605259](#)].
- [21] A.S. Dighe, T. Hurth, C.S. Kim and T. Yoshikawa, *Measurement of the lifetime difference of B_d mesons: Possible and worthwhile?*, *Nucl. Phys. B* **624** (2002) 377 [[hep-ph/0109088](#)].
- [22] HPQCD collaboration, *Lattice QCD matrix elements for the $B_s^0 - \bar{B}_s^0$ width difference beyond leading order*, *Phys. Rev. Lett.* **124** (2020) 082001 [[1910.00970](#)].
- [23] K.G. Chetyrkin, M. Misiak and M. Munz, *$|\Delta F| = 1$ nonleptonic effective Hamiltonian in a simpler scheme*, *Nucl. Phys. B* **520** (1998) 279 [[hep-ph/9711280](#)].
- [24] A. Hovhannisyanyan and U. Nierste, *Decay matrix of $B - \bar{B}$ mixing: Mixing of dimension-seven operators into dimension-six operators under renormalization*, [2511.17759](#).
- [25] P. Nogueira, *Automatic Feynman Graph Generation*, *J. Comput. Phys.* **105** (1993) 279.

- [26] M. Gerlach, F. Herren and M. Lang, *tapir: A tool for topologies, amplitudes, partial fraction decomposition and input for reductions*, *Comput. Phys. Commun.* **282** (2023) 108544 [2201.05618].
- [27] R. Harlander, T. Seidensticker and M. Steinhauser, *Complete corrections of $\mathcal{O}(\alpha\alpha_s)$ to the decay of the Z boson into bottom quarks*, *Phys. Lett. B* **426** (1998) 125 [hep-ph/9712228].
- [28] T. Seidensticker, *Automatic application of successive asymptotic expansions of Feynman diagrams*, in *6th International Workshop on New Computing Techniques in Physics Research: Software Engineering, Artificial Intelligence Neural Nets, Genetic Algorithms, Symbolic Algebra, Automatic Calculation*, 5, 1999 [hep-ph/9905298].
- [29] J.A.M. Vermaseren, *New features of FORM*, math-ph/0010025.
- [30] M. Tentyukov and J.A.M. Vermaseren, *The Multithreaded version of FORM*, *Comput. Phys. Commun.* **181** (2010) 1419 [hep-ph/0702279].
- [31] J. Kuipers, T. Ueda, J.A.M. Vermaseren and J. Vollinga, *FORM version 4.0*, *Comput. Phys. Commun.* **184** (2013) 1453 [1203.6543].
- [32] B. Ruijl, T. Ueda and J. Vermaseren, *FORM version 4.2*, 1707.06453.
- [33] T. van Ritbergen, A.N. Schellekens and J.A.M. Vermaseren, *Group theory factors for Feynman diagrams*, *Int. J. Mod. Phys. A* **14** (1999) 41 [hep-ph/9802376].
- [34] P. Reeck, V. Shtabovenko and M. Steinhauser, *B meson mixing at NNLO: technical aspects*, *JHEP* **08** (2024) 002 [2405.14698].
- [35] P. Maierhöfer, J. Usovitsch and P. Uwer, *Kira—A Feynman integral reduction program*, *Comput. Phys. Commun.* **230** (2018) 99 [1705.05610].
- [36] J. Klappert, F. Lange, P. Maierhöfer and J. Usovitsch, *Integral reduction with Kira 2.0 and finite field methods*, *Comput. Phys. Commun.* **266** (2021) 108024 [2008.06494].
- [37] F. Lange, J. Usovitsch and Z. Wu, *Kira 3: integral reduction with efficient seeding and optimized equation selection*, 2505.20197.
- [38] M. Fael, F. Lange, K. Schönwald and M. Steinhauser, *A semi-analytic method to compute Feynman integrals applied to four-loop corrections to the $\overline{\text{MS}}$ -pole quark mass relation*, *JHEP* **09** (2021) 152 [2106.05296].
- [39] M. Fael, F. Lange, K. Schönwald and M. Steinhauser, *Massive Vector Form Factors to Three Loops*, *Phys. Rev. Lett.* **128** (2022) 172003 [2202.05276].
- [40] M. Fael, F. Lange, K. Schönwald and M. Steinhauser, *Singlet and nonsinglet three-loop massive form factors*, *Phys. Rev. D* **106** (2022) 034029 [2207.00027].
- [41] M. Fael, F. Lange, K. Schönwald and M. Steinhauser, *Massive three-loop form factors: Anomaly contribution*, *Phys. Rev. D* **107** (2023) 094017 [2302.00693].
- [42] Ancillary files at: <https://www.ttp.kit.edu/preprints/2025/ttp25-054/>.

- [43] PARTICLE DATA GROUP collaboration, *Review of particle physics*, *Phys. Rev. D* **110** (2024) 030001.
- [44] K.G. Chetyrkin, J.H. Kuhn, A. Maier, P. Maierhofer, P. Marquard, M. Steinhauser et al., *Addendum to “Charm and bottom quark masses: An update”*, [1710.04249](#).
- [45] K. Chetyrkin, J.H. Kuhn, A. Maier, P. Maierhofer, P. Marquard, M. Steinhauser et al., *Precise Charm- and Bottom-Quark Masses: Theoretical and Experimental Uncertainties*, *Theor. Math. Phys.* **170** (2012) 217 [[1010.6157](#)].
- [46] R.J. Dowdall, C.T.H. Davies, R.R. Horgan, G.P. Lepage, C.J. Monahan, J. Shigemitsu et al., *Neutral B-meson mixing from full lattice QCD at the physical point*, *Phys. Rev. D* **100** (2019) 094508 [[1907.01025](#)].
- [47] A. Bazavov et al., *B- and D-meson leptonic decay constants from four-flavor lattice QCD*, *Phys. Rev. D* **98** (2018) 074512 [[1712.09262](#)].
- [48] C. Hughes, C.T.H. Davies and C.J. Monahan, *New methods for B meson decay constants and form factors from lattice NRQCD*, *Phys. Rev. D* **97** (2018) 054509 [[1711.09981](#)].
- [49] ETM collaboration, *Mass of the b quark and B -meson decay constants from $N_f=2+1+1$ twisted-mass lattice QCD*, *Phys. Rev. D* **93** (2016) 114505 [[1603.04306](#)].
- [50] HPQCD collaboration, *B-Meson Decay Constants from Improved Lattice Nonrelativistic QCD with Physical u, d, s, and c Quarks*, *Phys. Rev. Lett.* **110** (2013) 222003 [[1302.2644](#)].
- [51] LHCb collaboration, *Precise determination of the $B_s^0-\bar{B}_s^0$ oscillation frequency*, *Nature Phys.* **18** (2022) 1 [[2104.04421](#)].
- [52] HEAVY FLAVOR AVERAGING GROUP (HFLAV) collaboration, *Averages of b-hadron, c-hadron, and τ -lepton properties as of 2023*, [2411.18639](#).